



Petrogenetic constraints of the La Quinta Formation igneous rocks, Serranía del Perijá, northern Colombian Andes

Néstor Cano^{1,2*}, Juan Carlos Molano², Janeth Sepúlveda³

1. Programa de Posgrado en Ciencias de la Tierra, Universidad Nacional Autónoma de México.

2. Departamento de Geociencias, Universidad Nacional de Colombia, Bogotá, Colombia.

3. Servicio Geológico Colombiano, Bogotá, Colombia

* Corresponding author: nacano@unal.edu.co; nacano@comunidad.unam.mx.

ABSTRACT

The La Quinta Formation is a Triassic-Jurassic volcano-sedimentary unit exposed in Colombia and Venezuela, that crops out along both flanks of the Serranía del Perijá and in western Mérida Andes. It is composed of reddish mudstones and sandstones interbedded with basaltic-to-rhyolitic lava flows and ignimbrites. This succession is locally intruded by dacitic-rhyolitic hypabyssal bodies, felsic dikes and small monzodioritic intrusions. The volcanism recorded in La Quinta comprises the whole subalkaline compositional spectrum from basaltic andesites-alkali basalts (plagioclase-augite), though andesites-trachyandesites-dacites (plagioclase-augite- β quartz-amphibole) and rhyolites-alkali rhyolites (β quartz-sanidine-plagioclase-biotite). Magnetite, ilmenite, hematite, zircon and apatite are recurrent accessory phases and suggest dominant oxidized conditions (+1.2 Ni-NiO to hematite-magnetite buffers) in the magmas. Clinopyroxene and ilmenite-magnetite geothermobarometry suggest an early crystallization of the former (ca. 1120 °C and 4.6 kbar) in the middle portion of a normal-to-thickened continental crust (26-49 km), and later fractionation of the Fe oxides (ca. 720 °C). In addition, some samples exhibit calc-silicate alteration formed of hydrated grossular-andradite, epidote and zeolites in association with possible sediment-hosted stratiform copper occurrences. According to mineralogical and geochemical evidence, these rocks belong to a single comagmatic suite in which differentiation processes were driven by low-pressure fractional crystallization and middle-crustal assimilation. Moreover, these rocks exhibit geochemical features indicative of low degrees of partial melting of a spinel lherzolite (or an enriched source) in a hybrid setting between subduction-related arc and intracontinental rifting. Thus, we propose a mixed tectonic scenario in which subduction of the Farallon plate beneath western South America combined with transtensional tectonics resulting from the break-up of Pangea, generated volcanic activity with an inherited arc-signature behind (landward) the arc axis.

Keywords: Triassic-Jurassic igneous rocks; hybrid arc-rift magmatism; break-up of Pangea; petrogenesis; stratiform Cu deposits.

Consideraciones petrogenéticas de las rocas ígneas de la Formación La Quinta en la serranía del Perijá, porción norte de Los Andes colombianos

RESUMEN

La Formación La Quinta es una unidad volcano-sedimentaria del Triásico-Jurásico que aflora en ambos flancos de la serranía del Perijá y en la parte occidental de Los Andes de Mérida, en Colombia y Venezuela. Está conformada por capas de lodolita y arenisca rojiza intercaladas con lavas basálticas a riolíticas e ignimbritas. Esta sucesión está localmente intruida por cuerpos hipoabisales riolíticos-dacíticos, diques félsicos y stocks monzodioríticos. El volcanismo registrado en la Formación La Quinta abarca un rango composicional amplio en la serie subalcalina que incluye: basalto alcalino-andesita basáltica (plagioclasa+augita), andesita-traquiandesita-dacita (plagioclasa+augita+cuarzo+anfíbol) y riolita-riolita alcalina (cuarzo+sanidina+plagioclasa+biotita). Los minerales accesorios son magnetita, ilmenita, hematita, circón y apatito, lo que sugiere condiciones oxidantes en los magmas (desde +1.2 Ni-NiO hasta el campo de hematita-magnetita). Análisis de geotermobarometría en clinopiroxeno (~1120 °C y 4.6 kbar) indican que su cristalización ocurrió en la porción media de una corteza continental normal a engrosada (26-49 km), y precedió al fraccionamiento de ilmenita-magnetita (~720 °C). Adicionalmente, las rocas exhiben alteración de calcisilicatos (grosularia-andradita hidratada, epidota y ceolitas), en asociación con posibles depósitos cupríferos estrato-ligados. Las evidencias mineralógicas y geoquímicas halladas sugieren que estas rocas pertenecen a una suite comagmática donde los procesos de diferenciación estuvieron gobernados por la cristalización fraccionada a baja presión y la asimilación parcial de la corteza media. Asimismo, estas rocas se formaron a partir de grados de fusión parcial bajos en una lherzolita de espinela (o una fuente enriquecida) dentro de un ajuste tectónico suprasubducción de naturaleza híbrida entre un arco y un rift. De tal modo, en este artículo se propone un escenario tectónico mixto en el cual la placa Farallón subducía bajo la placa Suramericana al mismo tiempo que se generaban cuencas transtensionales ligadas al rompimiento de Pangea. De allí la existencia de la actividad volcánica con firma de arco en La Quinta, que estaba ubicada detrás del arco principal.

Palabras clave: Rocas ígneas triásicas-jurásicas; magmatismo híbrido de arco-rift; rompimiento de Pangea; petrogenesis; depósitos de cobre estrato-ligados.

Record
Manuscript received: 23/05/2021
Accepted for publication: 14/06/2022

How to cite item:
Cano, N., Molano, J. C., & Sepúlveda, J. (2022). Petrogenetic constraints of the La Quinta Formation igneous rocks, Serranía del Perijá, northern Colombian Andes. *Earth Sciences Research Journal*, 26(2), 139-156. <https://doi.org/10.15446/esrj.v26n2.95993>

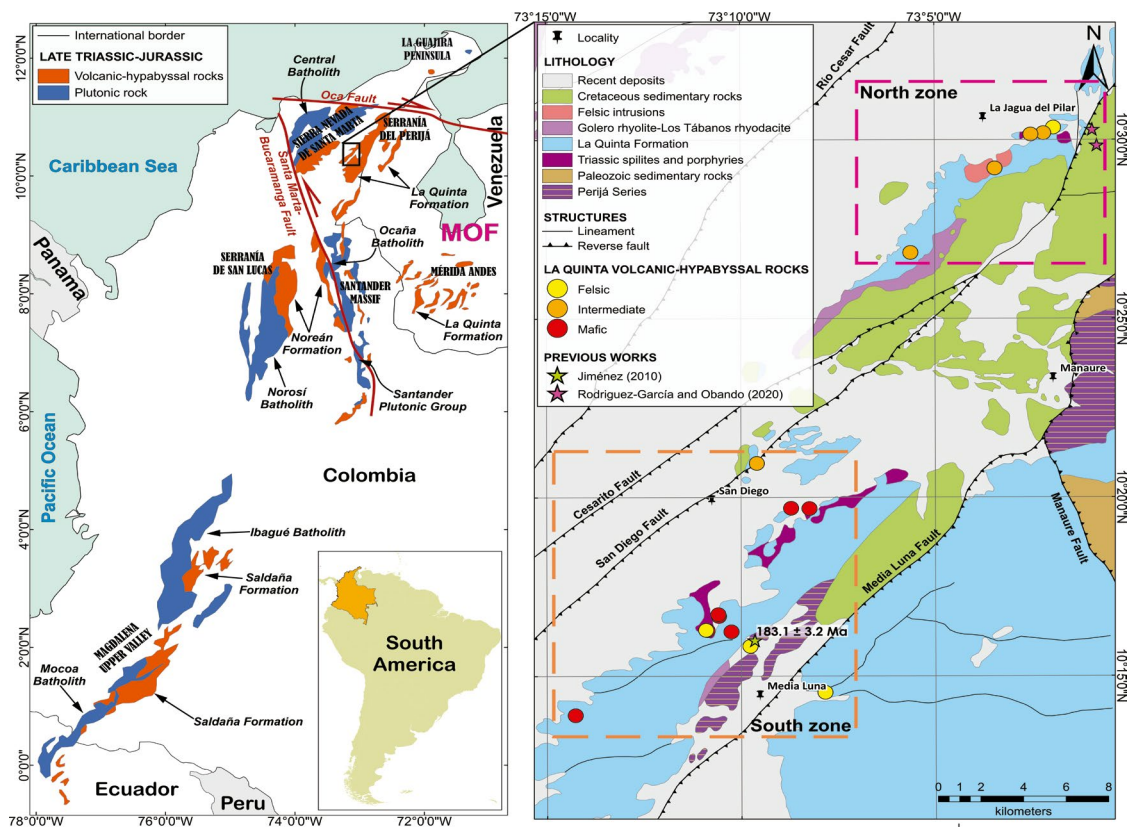


Figure 1. Location of the study area within the regional framework of latest Triassic-Jurassic magmatic rocks from Ecuador, Colombia and Venezuela. The area pertains to the Maracaibo Orogenic Float (MOF) (Cediel, 2019). The study zone is divided in two areas, one around the San Diego municipality (south) and the other near La Jagua del Pilar (north). Samples from previous studies are also depicted (Jiménez, 2010; Rodríguez-García & Obando, 2020), including a U-Pb zircon LA-ICP-MS age of 183.1 ± 3.2 Ma reported by Jiménez (2010) for a rhyolite. The location of major batholiths and volcanic-hypabyssal rocks was based on Maze (1984), van der Lelij et al. (2016), Nova et al. (2019), Bayona et al. (2020) and López-Isaza & Zuluaga (2020), and the geological basemap was taken from the 1:100.000 scale geological sheets 34-Valledupar and 27-Agustín Codazzi made by the Colombian Geological Survey (SGC, *Servicio Geológico Colombiano*) (Invemar et al., 2007; GRP Ltda., 2010).

1. Introduction

Latest Triassic-Jurassic (*ca.* 160-210 Ma) volcanic and plutonic rocks are widespread in discontinuous localities along the Colombian Andes (Figure 1), including the southern portion of the Eastern and Central Cordilleras, the Upper Magdalena Valley, Santander Massif, Serranía de San Lucas, Serranía del Perijá, Sierra Nevada de Santa Marta and La Guajira Peninsula (Bustamante et al., 2010; Leal-Mejía et al., 2019; Spikings et al., 2019; Bayona et al., 2020; López-Isaza & Zuluaga, 2020; Ramírez et al., 2020). These rocks display a wide compositional range in the sub-alkaline spectrum (basalt/gabbro to rhyolite/granite) (Rodríguez et al., 2018; Correa-Martínez et al., 2019; López-Isaza & Zuluaga, 2020; Rodríguez-García & Obando, 2020). The intrusive exponents are normally coarse quartzmonzonites, monzonites, monzogranites, granodiorites and minor diorites and gabbros (Spikings et al., 2019), whereas the volcanic and subvolcanic rocks include basaltic-rhyolitic lava flows, andesitic-rhyolitic tuffs, ignimbrites, epiclastic deposits and andesitic-dacitic hypabyssal bodies (Maze, 1984; Rodríguez-García et al., 2016; Correa-Martínez et al., 2019; Ramírez et al., 2020; Rodríguez-García & Obando, 2020). Additionally, they show consistent evidence of arc-related magmatism resulting from the subduction of the Farallon plate beneath the western margin of disassembling Pangea (Maze, 1984; Mojica & Kammer, 1995; Bustamante et al., 2010; Leal-Mejía, 2011; Villagómez et al., 2011; van der Lelij et al., 2016a; Rodríguez et

al., 2018; Correa-Martínez et al., 2019; Leal-Mejía et al., 2019; Spikings et al., 2019; Bayona et al., 2020; López-Isaza & Zuluaga, 2020; Rodríguez-García & Obando, 2020).

The present work will be centered in the La Quinta Formation, which outcrops in the Serranía del Perijá and the Mérida Andes (Figure 1) and is mostly constituted by Upper Triassic-Jurassic volcanic products interstratified with clastic sedimentary rocks (Champetier de Ribes et al., 1961; Forero, 1972; Maze, 1984; Gómez et al., 2010; Jiménez, 2010; González-Iregui et al., 2015; Rodríguez-García & Obando, 2020). This unit has been studied by several authors since the last century, partly because it hosts stratabound Cu±Ag mineralization concentrated in certain lava flows and sandstones with plants remains (Wokittel & Restrepo-Acevedo, 1955; Champetier de Ribes et al., 1961; Radelli, 1961; Pagnacco, 1962; Rodríguez, 1986; Jiménez, 2010; Ortega et al., 2012; González-Duran et al., 2017). Furthermore, the ubiquity of volcano-sedimentary successions ascribed to this unit in the westernmost Merida Andes and throughout the Serranía del Perijá (Figure 1) makes it a good natural “laboratory” to study several features of the Triassic-Jurassic, such as: paleoclimatology, tectonic arrangement during the break-up of Pangea, structural and depositional conditions, crustal thickness, nature of the magmatism, etc. (*e.g.*, Maze, 1984; Ostos et al., 2005; Langer et al., 2014; Nova et al., 2019).

Table 1. Location and field classification of the studied igneous rocks from the La Quinta Formation

Sample	P	E	L	Field classification	Latitude	Longitude	Northing	Easting
1163			X	Basalt	10.3281	-73.1373	1634067	1102979
1167	X		X	Rhyolite	10.2424	-73.1307	1624583	1103733
1223			X	Diorite	10.2712	-73.1812	1627761	1098191
1224	X	X	X	Basalt	10.2779	-73.1763	1628496	1098724
1225	X		X	Basalt	10.2787	-73.1765	1628590	1098699
1227	X		X	Ignimbrite	10.5057	-73.0323	1653751	1114418
1228				Andesite	10.5031	-73.0366	1653460	1113954
1229	X	X		Andesite	10.5025	-73.0420	1653392	1113356
1230	X	X		Andesite	10.4867	-73.0575	1651641	1111670
1231	X		X	Andesite	10.4474	-73.0937	1647276	1107718
1232	X		X	Andesite	10.3492	-73.1599	1636390	1100505
1233				Basalt	10.3282	-73.1452	1634078	1102118
1234	X		X	Rhyolite	10.2639	-73.1628	1626954	1100206
1235				Basalt	10.2707	-73.1709	1627703	1099317
1236			X	Basalt	10.2317	-73.2378	1623372	1092000
1237	X	X	X	Rhyolite	10.2714	-73.1818	1098128	1627780

E: EPMA, L: litho geochemistry, P: petrography. Northing and easting based on UTM-Magna_Colombia_Bogota.

As shown by Maze (1984), Gómez et al. (2010) and González-Iregui et al. (2015), the La Quinta Formation displays important facial changes due to abrupt variations in the locus (and type) of volcanism, structural complexity and geometry of intracontinental transtensional basins, and hence regional correlations are sometimes difficult to state. In addition, sparse geochemical and petrographic data are currently available for this unit in the central Perijá range (e.g., Jiménez, 2010; Saez-Paz, 2012; Rodríguez-García & Obando, 2020), and no electron probe micro-analyses (EPMA) neither geothermobarometric studies have been conducted in such rocks. For those reasons, this work focused on a narrow territory that extends from the San Diego municipality (Cesar Department), southern part, to La Jagua del Pilar (La Guajira Department) to the north, which comprises a segment of the western flank of the Perijá range (Figure 1) where La Quinta volcano-sedimentary rocks are extensively exposed in long hills with a characteristic reddish tint (Colmenares et al., 2007; Invemar et al., 2007; GRP Ltda., 2010). We centered on the volcanic rocks and hypabyssal bodies, which are one of the septentrional expressions of the Jurassic suprasubduction magmatism in the Colombian Andes. As a result, some petrologic features are described herein, which are supported on field observations (Table 1), petrography/metallography (Table 2), EPMA (Table 3a-b) and litho geochemical data (Table 4a-b). In the end, we propose a hybrid tectonic setting responsible for this magmatism, involving subduction and coeval intracontinental extension, as well as several evolutionary processes that were involved in its petrogenesis.

2. Geological setting

The Colombian Andes are divided into three mountain belts: the Western, Central and Eastern cordilleras. The latter has its northern termination in the Santander Massif, where it divides into the Mérida Andes, which continues to Venezuela with a northeast trend, and the Serranía del Perijá following a north-northeast orientation. The study zones are located in the central segment of the Perijá range within the Maracaibo Orogenic Float (Cediel, 2019), a triangular-shaped tectonic block that also encompasses the Mérida Andes, Santander Massif, Sierra Nevada de Santa Marta and the basement of Lake Maracaibo (Kellogg, 1984; Cediel, 2019).

The western flank of the Serranía del Perijá comprises metamorphic, igneous and sedimentary rocks with ages ranging from Paleozoic to Mesozoic (Colmenares et al., 2007; Invemar et al., 2007; GRP Ltda., 2010). In the study zones (Figure 1), the oldest unit is the Perijá Series (or undifferentiated Cambrian-Ordovician metasedimentites), which is exposed in discontinuous localities along a northeast general trend and consist of low-grade metasedimentites, mostly phyllites and quartzites (Forero, 1972; Invemar et al., 2007; Gómez et al., 2010). The Cachirí Group (Devonian) rests unconformably over the metamorphic basement and is dominated by sandstones and mudstones, with minor conglomerates at the base (Forero, 1972; Colmenares et al., 2007; Gómez et al., 2010). Moreover, the Carboniferous sedimentary rocks are mostly formed of conglomerates, sandstones and siliceous mudstones, with calcareous mudstones and limestones to the top (Gómez et al., 2010). The contact between the Carboniferous and Permian successions is difficult to establish since there is neither an unconformity nor obvious facial changes (Forero, 1972). Nevertheless, the Permian strata (Manaure Formation) is mainly represented by limestones with fusulinids, sandstones and mudstones (Wokittel & Restrepo-Acevedo, 1955; Forero, 1972; Gómez et al., 2010).

The oldest Mesozoic rocks are latest Triassic-early Jurassic basaltic to latitic lava flows included in the Triassic spilites (Tschanz et al., 1969; Colmenares et al., 2007; Invemar et al., 2007; Ramírez et al., 2020), which possibly belong to the same magmatic pulse as the La Quinta Formation volcanics. The youngest sedimentary record in the study areas is Cretaceous in age and corresponds to: 1) the Río Negro Formation, consisting of coarse-grained conglomerates and sandstones with minor mudstones, and 2) the undifferentiated shales and limestones, included by Gómez et al. (2010) in the Cogollo Group, which are composed of shales and fossiliferous limestones (Wokittel & Restrepo-Acevedo, 1955; Colmenares et al., 2007; Invemar et al., 2007; Gómez et al., 2010).

The La Quinta Formation was first introduced by Kündig (1938; in Forero, 1972) near the La Grita locality in the Táchira State (Venezuela), encompassing a thick (ca. 2.3 km) volcano-sedimentary and red-bed succession in between Permian and Cretaceous rocks that is extensively exposed in western Venezuelan Andes. In Colombia, the term was coined by Miller (1969; in Gómez

et al., 2010) in order to comprise Jurassic sedimentary rocks outcropping on the western flank of the Perijá range, the western basin of Ranchería and Cesar rivers and the Majuyura hill (norther termination of the Perijá range). After that, the term “La Quinta Formation” has been maintained and greatly used in both northernmost Colombian and western Mérida Andes (Champetier de Ribes et al., 1961; Radelli, 1961; Forero, 1972; Maze, 1984; Montaña, 2009; Gómez et al., 2010; Jiménez, 2010; Ortega et al., 2012; González-Iregui et al., 2015; van der Lelij et al., 2016a; López-Isaza & Zuluaga, 2020; Rodríguez-García & Obando, 2020).

Forero (1972) constructed a detailed stratigraphic column of this unit along the Manaure River (east of Manaure municipality) and defined four sets: 1) a normally graded succession of red conglomerates and sandstones with ignimbrites to the top; 2) fine-grained cross-bedded red and purple sandstones gradually interfingering with mudstones; 3) rhyolitic tuffs interbedded with sandstones and conglomerates; and 4) acidic volcanic products (rhyolites and ignimbrites) indicating a late flare-up in the volcanism. In addition, massive and vesicular basalts are present in some localities, sometimes hosting Cu mineralization (Gómez et al., 2010; Jiménez, 2010; Ortega et al., 2012; UNAL-SGC, 2014, 2020; González-Duran et al., 2017), and scarce small intrusions are also exposed (Maze, 1984; and references therein).

Depositional dynamics in La Quinta were strongly influenced by the extensional regime generated by the North and South American plates divergence, counterclockwise rotation of the Yucatán Block and seafloor spreading in the proto-Caribbean ocean (Bayona et al., 2020). Fluvial deposits contemporaneous with volcanic activity produced a hybrid succession of varying thicknesses (Forero, 1972; Gómez et al., 2010; González-Iregui et al., 2015), owing to the presence of intracontinental transtensional basins (narrow graben systems) (Maze, 1984; Ostos et al., 2005; van der Lelij et al., 2016a; Bayona et al., 2020), such as: Barquisimeto, Uribante and Machiques (Nova et al., 2019); the latter corresponding to the present-day Perijá range.

Several geochronological studies have been performed in the La Quinta Formation volcanic rocks in the Perijá range and Mérida Andes, defining a *ca.* 160-230 Ma (U-Pb in zircon and Ar-Ar in biotite) interval for the active supra-subduction magmatism recorded in this unit (Langer et al., 2014; González-Iregui et al., 2015; van der Lelij et al., 2016b; van der Lelij et al., 2016a; Nova et al., 2019; Rodríguez-García & Obando, 2020). According to Rodríguez-García and Obando (2020), the volcanism became progressively acidic with time and started with basaltic trachyandesites lava flows, then trachyandesites and dacites and finally the ignimbritic-rhyolitic flare-up. Furthermore, provenance analyses based on zircon LA-ICP-MS ages made by Montaña (2009) and Nova et al. (2019) in sandstones revealed four populations: 1) *ca.* 900-1300; 2) *ca.* 400-650; 3) *ca.* 250; and 4) *ca.* 180 Ma, leading to the authors to postulate the Santander Massif and Mérida Andes as the main sources of sediments. In addition, dinosaur remains (*Lesothosaurus* sp and *Tachiraptor admirabilis* gen. et sp. nov) (Barrett et al., 2008; Langer et al., 2014), conchostracans (*Estherida*) (Maze, 1984) and plant and fish (*Lepidotus*) remnants (Forero, 1972; and references therein) found in various segments of the succession suggest a wider range for sedimentation from Upper Triassic to Lower Cretaceous.

The ages presented by several authors for the La Quinta Formation in Colombia (*ca.* 165-188) (Jiménez, 2010; González-Iregui et al., 2015; Nova et al., 2019; Rodríguez-García and Obando, 2020) coincide with the Lower-Middle Jurassic ages reported in copious volcanoclastic units from other parts of the country, such as: 1) the Ipapure Rhyodacite (181-184 Ma) in the Guajira Peninsula (López-Isaza & Zuluaga, 2020; and references therein); 2) the Noreán Formation (175-192 Ma) in the northern Santander Massif and Serranía de San Lucas (Correa-Martínez et al., 2019); 3) the Guatapurí and Corual Formations, Golero Rhyolite, Los Tábanos Rhyodacite and ignimbritic units (e.g., Caja de Ahorros, La Paila and Los Clavos) (165-195 Ma) in the Sierra Nevada de Santa Marta (Ramírez et al., 2020); and are slightly older than the 4) Saldaña Formation (146-189 Ma) and Pitalito volcanites (168-172 Ma) in the Central Cordillera and Upper Magdalena Valley (Rodríguez-García et al., 2016; Rodríguez-García, 2018; López-Isaza & Zuluaga, 2020). Mojica & Kammer (1995) named this period of intense volcanic activity as the “Saldaña Volcanism”. Besides, it is worth noting that the late Triassic-Jurassic magmatic pulses are not restricted to Colombia; instead, they are present in numerous localities from North, Central and South America (Maze, 1984; Martini & Ortega-Gutiérrez, 2018; Bayona et al., 2020).

3. Methods

A total of sixteen samples of volcanic rocks from the La Quinta Formation were collected in two zones (north and south) of the western flank of the Serranía del Perijá (Figure 1, Table 1). We collected lithologies with contrasting compositions (basalts, andesites, rhyolites, rhyolitic tuffs and diorites) in order to observe evolutionary trends. Hydrothermally altered and/or weathered rocks were avoided; only the sample 1163, which exhibits visible hydrothermal alteration, was analyzed for comparison purposes. Ten polished thin sections were studied with a petrographic microscope equipped with transmitted and reflected light. Rock classification was performed following LeMaitre et al. (2002) and mineral abbreviations were taken from Whitney & Evans (2010).

Four samples were chosen for further electron microprobe analyses (spots and compositional maps) to characterize magmatic and alteration mineral phases. Mineral compositions were obtained using the JEOL JXA-8230 electron probe microanalyzer of the *Departamento de Geociencias (Universidad Nacional de Colombia)*, at 15 and 20 keV for silicates and oxides, respectively. The analytical programs and standards for ilmenite and magnetite were kyanite (Si, TAP, $K\alpha$), kyanite (Al, TAP, $K\alpha$), Mg oxide (Mg, TAP, $K\alpha$), pure Zn (Zn, TAP, $L\alpha$), Ti foil (Ti, PETJ, $K\alpha$), diopside (Ca, PETJ, $K\alpha$), pure Ni (Ni, LIFH, $K\alpha$), hematite (Fe, LIFH, $K\alpha$), pure Mn (Mn, LIFH, $K\alpha$), Cr oxide (Cr, LIFH, $K\alpha$), pure V (V, LIFH, $K\alpha$); pyroxene: sodalite (Na, TAP, $K\alpha$), forsterite (Mg, TAP, $K\alpha$), omphacite (Al, TAP, $K\alpha$), pyrope (Si, TAP, $K\alpha$), ilmenite (Ti, PETJ, $K\alpha$), diopside (Ca, PETJ, $K\alpha$), orthoclase (K, PETH, $K\alpha$), fayalite (Fe, LIFH, $K\alpha$), spessartine (Mn, LIFH, $K\alpha$), Cr oxide (Cr, LIFH, $K\alpha$); plagioclase: albite (Na, TAP, $K\alpha$), hornblende (Mg, TAP, $K\alpha$), orthoclase (Al, TAP, $K\alpha$), orthoclase (Si, TAP, $K\alpha$), ilmenite (Ti, PETJ, $K\alpha$), anorthite (Ca, PETJ, $K\alpha$), orthoclase (K, PETH, $K\alpha$), fayalite (Fe, LIFH, $K\alpha$), spessartine (Mn, LIFH, $K\alpha$), Cr oxide (Cr, LIFH, $K\alpha$); garnet: sodalite (Na, TAP, $K\alpha$), pyrope (Mg, TAP, $K\alpha$), orthoclase (Al, TAP, $K\alpha$), pyrope (Si, TAP, $K\alpha$), ilmenite (Ti, PETJ, $K\alpha$), diopside (Ca, PETJ, $K\alpha$), orthoclase (K, PETH, $K\alpha$), fayalite (Fe, LIFH, $K\alpha$), spessartine (Mn, LIFH, $K\alpha$), Cr oxide (Cr, LIFH, $K\alpha$); zeolites: albite (Na, TAP, $K\alpha$), hornblende (Mg, TAP, $K\alpha$), orthoclase (Al, TAP, $K\alpha$), albite (Si, TAP, $K\alpha$), ilmenite (Ti, PETJ, $K\alpha$), anorthite (Ca, PETJ, $K\alpha$), orthoclase (K, PETH, $K\alpha$), fayalite (Fe, LIFH, $K\alpha$), spessartine (Mn, LIFH, $K\alpha$), Cr oxide (Cr, LIFH, $K\alpha$); epidote and sodalite (Na, TAP, $K\alpha$), hornblende (Mg, TAP, $K\alpha$), hornblende (Al, TAP, $K\alpha$), hornblende (Si, TAP, $K\alpha$), ilmenite (Ti, PETJ, $K\alpha$), diopside (Ca, PETJ, $K\alpha$), hornblende (K, PETH, $K\alpha$), hornblende (Fe, LIFH, $K\alpha$), spessartine (Mn, LIFH, $K\alpha$), Cr oxide (Cr, LIFH, $K\alpha$).

Geothermobarometric calculations were performed using the clinopyroxene-only thermobarometer for mafic-to-intermediate magmatic systems (Nimis, 1995; Wang et al., 2021) and the ilmenite-magnetite (ILMAT) thermometer (Lepage, 2003).

Major and trace elements of eleven samples were analyzed at ALS Chemex Laboratories by X-ray fluorescence (XRF), inductively coupled plasma mass spectrometry (ICP-MS) and inductively coupled plasma atomic emission spectroscopy (ICP-AES), following the procedures explained in ALS-Chemex (2022). All the analyzed rocks were classified on an anhydrous basis and the geochemical data were plotted using the GCDkit R-based software.

4. Results

Field work

In the study area, most of the La Quinta Formation is represented by a thick succession of reddish-burgundy fine-grained sandstones, mudstones and minor conglomerates interbedded with felsic-to-mafic volcanic and volcanoclastic horizons of variable thicknesses (>3 m).

The volcanic and volcanoclastic beds are mainly formed of basaltic lava flows, small andesitic-rhyolitic stocks or domes and ignimbrites. Mafic flows (samples 1163, 1224, 1225, 1233, 1235 and 1236) were only observed in the south zone (Figure 1) and consist of massive basalts (Figure 2A) with aphanitic to porphyritic texture composed of small plagioclase phenocrysts (<1 mm) surrounded by a dark gray matrix. These rocks may be moderately to highly vesiculated (Figure 2B), especially to the top of the flows, having amygdules filled with epidote (Figure 2C), zeolites, quartz, carbonates and/or copper minerals. Conversely, andesitic lava flows and porphyries are more common in the north zone (nearby La Jagua del Pilar) and the northern portion of the south zone

Table 2. Main petrographic features of the volcanic rocks from the La Quinta Formation.

Sample	Percentage (%)								Accessory	Alteration	Petrographic classification
	Qz	Pl	Sa	LF	Mx	Bt	Cpx	Ol			
1229	-	54.7	-	-	-	-	7.7	-	Ap, Hem, Mag, Ccp Brn	Arc, Chl, Ser	Andesite
1230	-	63.2	-	-	-	-	-	-	Mag, Ilm	Chl, Zeo, Arc, Cb, Ep	Andesite
1231	1.6	79.5	-	-	-	-	-	-	Zrn, Ap, Hem	Chl, Arc, Ep, Ser	Andesite
1232	-	38.5	-	0.3	35.6	4.4	-	-	Zrn, Ap, Mag, Ilm	Cb, Ser, Chl	Andesite
1224-1225	-	66.5	-	-	-	-	8.6	tr	Mag, Ilm	Grt, Srp, Chl, Ep, Cb	Basalt
1227	56.3	12.0	2.4	-	-	0.4	-	-	Zrn, Mag	Arc, Chl, Cb, Ep	Ignimbrite
1234	4.0	8.0	3.0	-	51.0	1.0	-	-	Zrn, Mag	Arc, Ser, Cb, Zeo	Rhyolite
1237	18	25.5	-	-	-	-	-	-	Mag	Arc, Ep, Zeo	Dacite (?)
1167	4.6	13.6	6.0	-	62.4	0.3	-	-	Zrn, Ap	Cb, Ser, Ep	Rhyolite

Ap: apatite, Arc: clay minerals, Brn: bornite, Bt: biotite, Cb: carbonate, Ccp: chalcopyrite, Chl: chlorite, Cpx: clinopyroxene, Ep: epidote, Hem: hematite, Ilm: ilmenite, Sa: alkali feldspar (sanidine), LF: lithic fragments, Mag: magnetite, Mx: matrix, Ol: olivine, Pl: plagioclase, Qz: quartz, Ser: sericite, tr: traces, Zeo: zeolites, Zrn: zircon.

(Figure 1). The andesitic flows (samples 1230 and 1231) (Figure 2D-E) display porphyritic-trachytic texture and are constituted by plagioclase phenocrysts of up to 1 cm, often altered to sericite and clay minerals, with minor amphibole and biotite phenocrysts, all of them embedded in a microcrystalline matrix.

Andesites with medium- to fine-grained porphyritic texture (samples 1229 and 1232) were found in scarce localities to the southeast of La Jagua del Pilar and northeast of San Diego (Figure 1). They normally appear in homogeneous outcrops around isolated hills that show no relationship with the red-beds and are formed of plagioclase and pyroxene phenocrysts surrounded by a light grey crystalline matrix. In a similar fashion, rhyolites outcropping south of San Diego (sample 1234) and east of Media Luna (sample 1167) (Figure 2F) are relatively confined with respect to sedimentary and volcanoclastic rocks, and display a characteristic porphyritic texture marked by bipyramidal quartz, alkali feldspar and plagioclase phenocrysts embedded in a light purple fine-grained matrix. Given the distribution and features of such rhyolites and porphyritic andesites, they were interpreted as being part of domes and stocks; however, the contacts with the enclosing rocks were not observed.

A dioritic stock (sample 1223) was found south of San José (Figure 1), constituted by fine-grained plagioclase and amphibole, which hosts a leucocratic microcrystalline dike (sample 1237), *ca.* 35 cm wide, with reduced lateral continuity (<1.5 m). Finally, felsic tuffs (sample 1227) were only recognized east of La Jagua del Pilar, formed of bipyramidal quartz and small biotite phenocrysts with rare small burgundy lithic fragments (sedimentary rocks).

It is worth mentioning that the relationship between the sedimentary rocks and lava flows was only visible in one outcrop (sample 1230) (Figure 2D) and corresponds to interstratifications in which fine-grained clastic rocks do not show contact thermal effects (Figure 2D). In addition, Cu occurrences formed of malachite, azurite, chrysocolla, cuprite, chalcopyrite, bornite and covellite, are remarkable in some localities (*e.g.*, samples 1163 and 1223).

Petrography

In the study zones, the La Quinta Formation comprises a series of basaltic-to-andesitic lava flows interbedded with ignimbrites and sandstones, as well as porphyritic rhyolites and andesites and minor dioritic intrusions. Most of the analyzed samples exhibit fine-grained porphyritic texture and have mafic, intermediate and felsic compositions (Table 2). Moreover, as indicated below, these rocks display modest hydrothermal and supergene alteration except for the sample 1163, which is altered to a calc-silicate assemblage of epidote-prehnite-chlorite-calcite.



Figure 2. Field features of the La Quinta Formation volcanic rocks in the study areas. A. Massive basalt (sample 1236). B. Highly vesiculated basalt. C. Epidote (Ep) amygdules in basalt. D. Red-violet mudstones interbedded with an andesitic lava flow (sample 1230). E. Detail of the andesitic flow from D., showing porphyritic and fluidal texture demarcated by plagioclase (Pl) phenocrysts. F. Probable rhyolitic dome (sample 1234).

Mafic rocks

Two samples with different degrees of hydrothermal alteration were collected in a basaltic flow from south of San Diego: sample 1224 (fresh basalt) and 1225 (oxidized and altered basalt). Both rocks display fine-grained

holocrystalline-trachytic and ophitic texture formed of zoned plagioclase (76.0%) and clinopyroxene (11.0%) (Figure 3A-B). Additionally, scant olivine (<1.0%) replaced by serpentine and chlorite was observed, along with ilmenite and magnetite as accessory minerals (Figure 3C). The sample 1225 shows incipient calc-silicate hydrothermal alteration that appears disseminated, as patches and substituting olivine and clinopyroxene. This alteration is composed of chlorite, epidote, carbonates and poorly crystallized garnet. Nevertheless, González-Duran et al. (2017) reported more complex hydrothermal assemblages often linked to the Cu mineralization in other areas of the south zone, including epidote, K-rich feldspar, albite, prehnite, pumpellyite, etc. (Figure 3D).

Intermediate rocks

Andesites (samples 1229, 1230, 1231 and 1232) are the most common lithology in the studied samples. These rocks are largely constituted by euhedral plagioclase phenocrysts (30.0-35.0%) or microlites (25.0-45.0%) surrounded by a devitrified matrix (35.0%), and variable quantities of clinopyroxene (8.0%), biotite (4.0%), magnetite (3.0%), ilmenite (2.0%), hematite (1.5-2.0%), quartz (1.5%), lithic fragments (*ca.* 0.3%), apatite, zircon and scarce copper sulfides (Figure 4A-E). Plagioclase crystals normally develop polysynthetic twinning (albite and pericline), while clinopyroxene manifests simple twinning, pale greenish tint and second order interference colors (Figures 4C). Furthermore, sample 1232 hosts two types of lithic fragments: 1) very fine-grained sandstones, composed of sub-rounded quartz grains embedded in a dark muddy matrix; and 2) possible tonalite fragments with holocrystalline texture defined by quartz and plagioclase. Magnetite, ilmenite and primary hematite are common, the former two oxides forming exsolution lamellae (Figure 2D-E). Additionally, chalcocopyrite replaced by bornite was locally observed.

Zeolites (8%), carbonates (2-10%), epidote (1.0%), sericite (5.0%) and chlorite (2-15%) are uncommon and are observed as fillings and veinlets (Figure 4F), evidencing discrete hydrothermalism. On the other hand, clay minerals and iron oxides are a recurrent product of supergene alteration of plagioclase and amphiboles. In the sample 1230, zeolites were classified as stilbite given that they display medium relief, first order interference colors, negative biaxial interference figure with reduced 2V angle and radial habit (Figure 4F). Epidote normally appears as small aggregates of high relief, pale yellowish tint and third order birefringence, and hence was typified as pistacite; zoisite and clinzoisite were also identified.

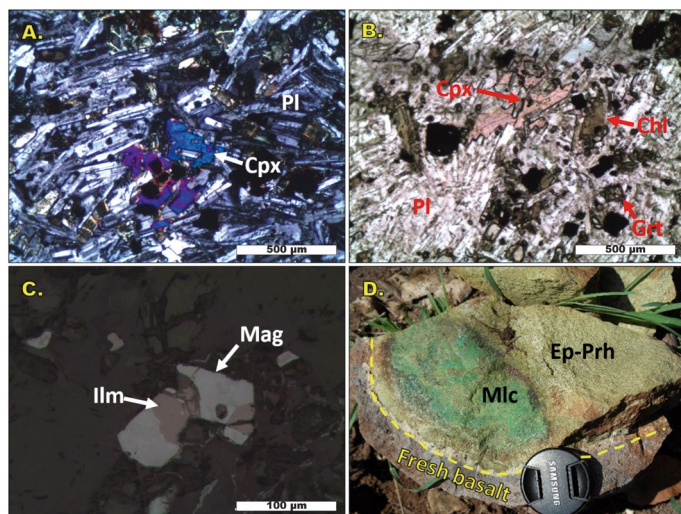


Figure 3. Mineralogy and textures of basaltic rocks from the La Quinta Formation. A-B. Photomicrographs of the general appearance, characterized by plagioclase (Pl) with trachytic texture and plagioclase-clinopyroxene (Cpx) intergrowths (ophitic texture). Notice the presence of chlorite (Chl) and ill-crystallized garnet (Grt) formed by hydrothermal alteration. C. Ilmenite (Ilm) associated with magnetite (Mag). D. Pervasive calc-silicate alteration of epidote (Ep) and prehnite (Prh) concentrated in the core of a basalt, surrounded by an unaltered carapace. Malachite (Mlc) patches produced by oxidation of native copper.

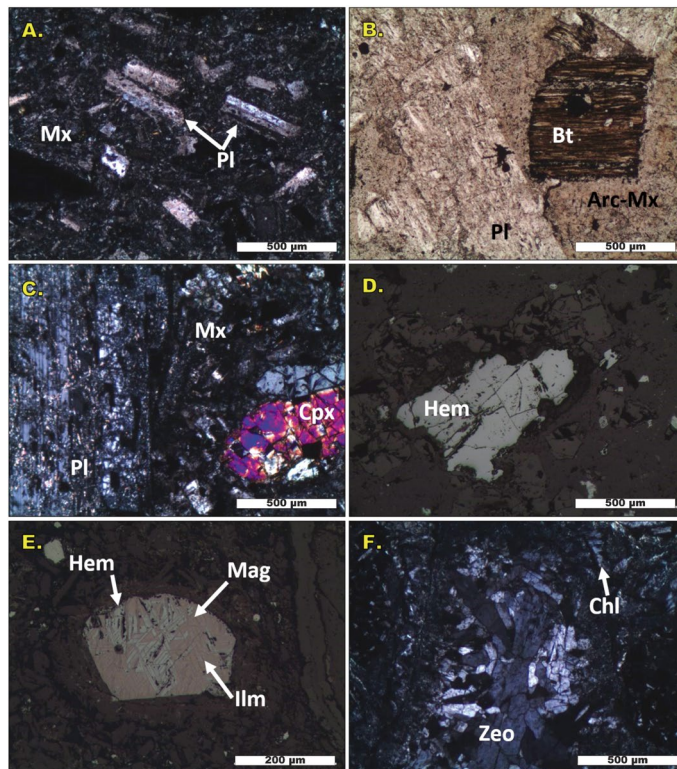


Figure 4. Mineralogy and textures of andesitic rocks from the La Quinta Formation. A-C. Plagioclase (Pl), biotite (Bt) and clinopyroxene (Cpx) phenocrysts surrounded by a fine-grained microlitic matrix (Mx) that is partly argillized. D-E. Hematite (Hem) and magnetite (Mag) crystals (accessory minerals), the latter is replaced by hematite as patches and shows geometric ilmenite (Ilm) exsolution lamellae. F. Zeolites (Zeo) fillings and chlorite (Chl) patches within the microcrystalline matrix.

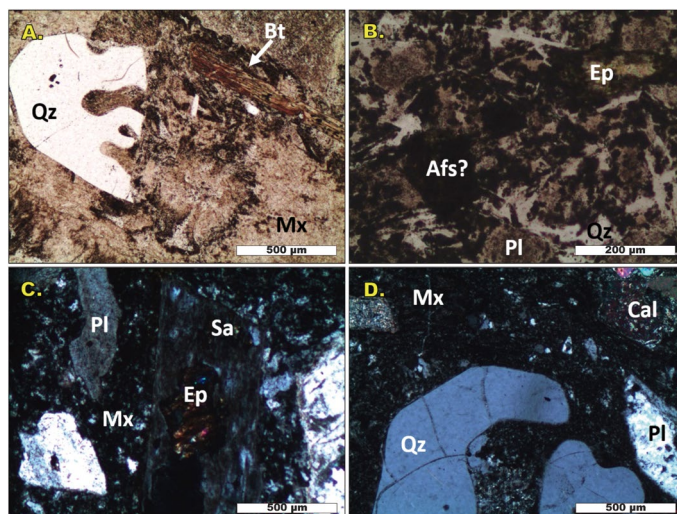


Figure 5. Mineralogy and textures of rhyolitic rocks from the La Quinta Formation. A. Rhyolitic ignimbrite formed of β -quartz (Qz) phenocrysts with embayments and biotite (Bt) embedded in a cryptocrystalline devitrified matrix (Mx) with discrete argillic alteration. B. Granophyric texture (?) in the felsic dike, defined by plagioclase (Pl), quartz and, possibly, alkali feldspar (Afs?). Epidote (Ep) pseudomorphs after mafic minerals are also present. C. Sanidine (Sa) and plagioclase phenocrysts surrounded by a fine-grained holocrystalline matrix. Small epidote patches. D. Rhyolite with embayed β -quartz phenocrysts surrounded by a devitrified groundmass. Notice the presence of secondary calcite (Cal) patches.

Felsic rocks

This group is mainly represented by rhyolites (samples 1167 and 1234), ignimbrites (samples 1227) and one felsic dike (sample 1237). The ignimbrite shows porphyritic texture with advanced devitrification and, locally, eutaxitic texture demarcated by *fiammes*. They are constituted by phenocrysts of β -quartz (13.0%), sanidine (3.0%) and plagioclase (12.0%), with minor zircon, biotite, magnetite and lithic fragments (Figure 5A). Glass shards and spherulites are common and quartz generally develops resorption embayments (Figure 5A).

The felsic dike has a diffuse porphyritic and apparent granophyric texture and is entirely composed of complex intergrowths of plagioclase (25%), quartz (18%) and a highly argillized mineral (alkali feldspar? (Figure 5B).

Rhyolites display porphyritic texture and are composed of large (>2 mm) plagioclase (8-14%), quartz (4%), sanidine (3-6%) and biotite (1.0%) phenocrysts, and minor amounts of zircon, magnetite and apatite crystals, all embedded within a devitrified cryptocrystalline matrix (Figures 5C-D). These rocks may host lithic fragments of granitoids with granular texture, formed of quartz, orthoclase and plagioclase. Besides, perthitic sanidine was observed in one of the samples.

Felsic rocks normally show mild hydrothermal alteration expressed as patches and partial replacements of mafic minerals (e.g., amphibole and biotite), and is represented calcite-epidote-chlorite-quartz-sericite-zeolites assemblages (propylitic alteration) (Figure 5C-D). In contrast, supergene alteration appears as advanced substitutions of feldspars phenocrysts, magnetite and the glassy matrix by clay minerals and earthy iron oxides.

Microchemical analyses

Microchemical analyses were carried out in primary (plagioclase, pyroxene, ilmenite and magnetite) and hydrothermal (epidote, zeolites and garnet) mineral phases. The results are summarized in Table 3a-b.

Plagioclase characterization was challenging in most of the samples due to supergene alteration of clay minerals and sericite (Figure 4A-C and 5C). However, unaltered plagioclase crystals in a basalt (sample 1224) (Figure 3A-B) exhibit normal zoning (Figure 6), defined by a Ca-rich core (An_{81}) and progressively Ca-poorer rims (An_{45-67}).

Table 3a. Electron microprobe quantitative results in magmatic minerals from the La Quinta Formation volcanic rocks. Concentrations are given in wt.%.

Sample	Ilmenite		Mag	Plagioclase			Clinopyroxene		
	1224	1224		C	R	B	1224	1224	1229
SiO ₂	0.00	0.00	0.00	50.81	55.48	61.00	52.36	52.35	52.74
TiO ₂	48.69	48.65	6.91	0.00	0.01	0.00	0.69	0.59	0.62
Al ₂ O ₃	0.00	0.00	0.09	31.76	27.94	24.30	0.00	0.00	0.67
FeO*	-	-	-	0.49	0.57	0.41	11.66	11.86	11.38
Fe ₂ O ₃	7.8	10.3	52.90	-	-	-	-	-	-
Cr ₂ O ₃	0.03	0.03	0.38						
FeO	37.9	37.9	36.50	-	-	-	-	-	-
MnO	5.72	5.71	0.06	0.00	0.00	0.00	0.37	0.35	0.28
MgO	0.02	0.02	0.10	0.00	0.00	0.00	14.28	13.91	14.92
CaO	0.05	0.05	0.05	13.66	10.04	5.77	17.99	18.21	17.92
Na ₂ O	0.00	0.00	0.00	3.56	5.51	7.75	0.33	0.35	0.39
K ₂ O	0.00	0.00	0.00	0.17	0.39	0.91	0.00	0.00	0.00
V ₂ O ₃	0.48	0.47	0.86	0.17	0.39	0.91	0.00	0.00	0.00
Σ	100.69	103.13	97.85	100.45	99.94	100.14	97.68	97.62	98.92
Cations	3 O		4 O	8 oxygens			6 oxygens		
Si	0.00	0.00	0.00	2.30	2.51	2.72	2.00	2.00	2.02
Ti	0.95	0.93	0.20	0.00	0.00	0.00	0.02	0.02	0.02
Al	0.00	0.00	0.00	1.70	1.49	1.28	0.00	0.00	0.03
Fe ²⁺ tot	-	-	-	0.02	0.02	0.01	0.37	0.38	0.36
Fe ³⁺	0.15	0.12	1.21	-	-	-	-	-	-
Fe ²⁺	0.81	0.78	1.58	-	-	-	-	-	-
Mn	0.13	0.12	0.00	0.00	0.00	0.00	0.01	0.01	0.01
Mg	0.00	0.00	0.00	0.00	0.00	0.00	0.81	0.79	0.85
Ca	0.00	0.00	0.00	0.66	0.49	0.28	0.74	0.75	0.74
Na	0.00	0.00	0.00	0.31	0.48	0.67	0.02	0.03	0.03
K	0.00	0.00	0.00	0.01	0.02	0.05	0.00	0.00	0.00
Σ	2.04	1.95	2.99	5.00	5.01	5.01	3.97	3.98	4.06

B = border; C = core, Mag = magnetite, R = rim, tot = total. Recalculated Fe₂O₃ and FeO in magnetite and ilmenite following Carmichael (1967).

Table 3b. Electron microprobe results in hydrothermal minerals from the La Quinta Formation volcanic rocks. Concentrations are given in wt.%.

	Grt	Zeolites		Ep
wt.%	1224	1230	1237	1237
SiO ₂	35.81	56.43	39.26	38.59
TiO ₂	0.30	0.00	0.00	0.00
Al ₂ O ₃	7.46	22.43	23.84	23.89
FeO	16.99	0.46	5.22	9.54
MnO	0.18	0.01	0.08	0.07
MgO	0.14	0.00	3.27	0.07
CaO	32.89	11.54	22.48	21.76
Na ₂ O	0.00	0.05	0.01	0.10
K ₂ O	0.00	0.15	0.00	0.01
Σ	93.77	91.07	94.16	94.03

Ep = epidote, Grt = garnet.

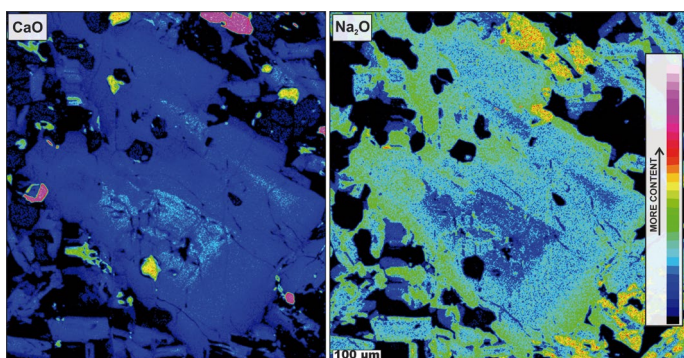


Figure 6. Calcium (left) and sodium (right) oxides compositional maps of a plagioclase crystal from a basalt (sample 1224). A normal zoning is observed, with Ca-rich core and progressive Na-richer rims. The color scalebar imply relative amounts, being pink/white higher concentration of Na₂O or CaO.

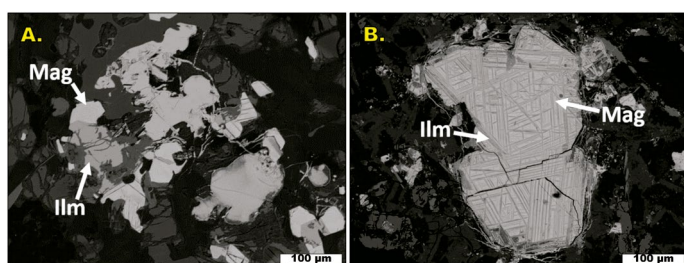


Figure 7. Backscattered electron images of magnetite (Mag) and ilmenite (Ilm). Ilmenite is characterized by a duller gray tint compared to magnetite.

Clinopyroxene is common in basalts and andesites, in the former displaying ophitic texture (Figure 3A). This mineral was classified as augite (En₄₁-43Fs₁₈-19Wo₃₇-38) following Morimoto (1988).

Hydrothermal alteration minerals, such as epidote, Ca-zeolites and garnet (Adr₇₀Gr_{s30}) yielded important contents of Ca (Table 3b), which agrees with the general calc-silicate assemblage recognized petrographically (Figure 3 and 5C). The fact that their summatory in quantitative analyses does not exceed 95 wt.% may be caused by the existence of variable amounts of water in the crystalline lattice of these minerals.

Magnetite is very common in all the studied samples and is closely related to ilmenite (Figure 3C and 7A); the latter is generally found as exsolution lamellae (Figure 4E and 7B). These crystals are disseminated in

association with other primary minerals, indicating a magmatic origin that was also suggested by enrichments in TiO₂ (7.5 wt.%), Cr₂O₃ (0.4 wt.%) and Nb₂O₃ (0.05 wt.%) (Nadoll et al., 2014).

Geothermobarometry

Using the ilmenite-magnetite (ILMAT) thermometer proposed by Lepage (2003), crystallization temperature and oxygen fugacity conditions were estimated for one of the basalts (sample 1224). It is essential to state that: 1) ilmenite exsolutions were avoided, since they are not in equilibrium with the hosting magnetite; and 2) the diagram of Bacon and Hirschmann (1988) (not shown) was used to confirm that equilibrium conditions were achieved during the crystallization of the ilmenite-magnetite pair, usually marked by a linear tendency intersecting close to the origin of the diagram. Thus, temperature and oxygen fugacity values of 700-736°C and *ca.* +1.2 NNO were obtained.

The clinopyroxene-only thermobarometer presented by Nimis (1995) and Wang et al. (2021) for basaltic-to-dacitic suites was applied to the same sample. Clinopyroxene in this rock yielded crystallization temperatures and pressures of 1118-1122 ± 36.6 °C and 4.5-4.7 ± 1.6 kbar. Assuming an andesitic composition for the bulk continental crust with a mean density of 2.6 g/cm³ (Klein and Johnson, 1983; Rudnick and Gao, 2003), the depth of crystallization varied between 17-19 km.

Whole-rock geochemistry

A total of eleven samples (Table 1), including basaltic andesites-trachyandesites (n: 3), dacites (n: 2), rhyolites (n: 2) and one monzodiorite, one ignimbrite and one felsic dike were selected for litho-geochemical analyses, and the results are summarized in Table 4a-b. According to the petrographic and geochemical features, these rocks were divided into three groups: felsic (rhyolites, ignimbrite and the leucocratic dike; SiO₂: 73.6-77.7 wt.%), intermediate (dacites, SiO₂: 64.0-66.1 wt.%) and mafic (basaltic andesites and trachyandesites, SiO₂: 49.0-58.3 wt.%) and will be accordingly referred hereafter. Overall, the samples present low values of LOI (0.9-3.1 wt.%) and were classified on an anhydrous basis; except for the sample 1163 (LOI = 7.4 wt.%), which was labeled as “altered basalt” and highlighted in the diagrams because it showed the strongest hydrothermal alteration in hand specimen. Additionally, geochemical data published by Jiménez (2010) and Rodríguez-García and Obando (2020) for the La Quinta Formation volcanic rocks nearby the study areas were incorporated in the mafic (basaltic trachyandesites, andesites and trachyandesites) and felsic groups (rhyolites), based on similarities in geochemical signatures with our samples.

In the alteration box plot by Large et al. (2001) (Figure 8A) all the samples appear in the “least altered box” except for one rhyolite (sample 1234), but this is due to its high concentration of K₂O (*ca.* 6.6 wt.%) in alkali feldspar phenocrysts and probably in the matrix. Nevertheless, this sample plots close to the 1:1 linear regression expected for low-altered rocks (Figure 8A). Although hydrothermal and supergene alterations were apparently not severe enough to modify the primary signature of the volcanic rocks, we preferred classification and geotectonic diagrams based on immobile or less mobile incompatible elements.

The studied volcanic rocks display a wide range of composition from alkali basaltic/basaltic to rhyolitic and plot along a linear trend near the limit between the fields of calc-alkaline series and high-K calc-alkaline and shoshonite series (Figure 8B-C) (Pearce, 1996; Hastie et al., 2007). The samples straddle the metaluminous and peraluminous fields in the Shand's index diagram (Figure 8D): 1) mafic rocks are metaluminous and plot close to the limit with the peraluminous field; 2) intermediate rocks are slightly peraluminous, and 3) the felsic rocks are moderately to highly peraluminous. However, the felsic dike and altered basalt have a contrasting behavior, lying within the metaluminous box and close to the limit with the peralkaline field.

Harker diagrams depict continuous negative trends in FeO*, CaO, MgO, P₂O₅ and TiO₂ (Figure 9) with respect to SiO₂, suggesting: 1) the early crystallization of clinopyroxene, olivine, magnetite, ilmenite, apatite and, partly, plagioclase (Winter, 2014), which are minerals especially abundant in the studied mafic rocks (Figure 3A-C); and 2) that the rocks are part of a single igneous suite (Gill, 2010; Frost and Frost, 2014). At low SiO₂, Al₂O₃ exhibits a positive trend (early crystallization of Fe-Mg-Ti phases) that switches at *ca.* 55 wt.% of SiO₂, marking the moment at which plagioclase fractionation became significant in the differentiation process. In contrast, K₂O and Na₂O display some degree of scatter (Figure 9). The former shows an ill-defined

positive correlation with increasing SiO₂ (late fractionation of alkali-felspar and biotite), whereas the latter has an opposite behavior. Moreover, excluding the felsic dike, Zr decreases compared to SiO₂ in all the studied samples and those analyzed by Jiménez (2010), even though zircon crystals are common in felsic

and intermediate rocks (Table 2) but apparently absent in mafic exponents. This may be due to an early fractionation of very fine-grained zircon or baddeleyite crystals, difficult to observe petrographically.

Table 4b. Trace and rare earth elements of the La Quinta Formation igneous rocks. Values are expressed in ppm.

Sample	1163	1167	1223	1224	1225	1227	1231	1232	1234	1236	1237
Li	10.0	10.0	20.0	20.0	20.0	20.0	10.0	20.0	20.0	20.0	10.0
Sc	16.0	3.0	12.0	16.0	15.0	2.0	9.0	8.0	2.0	13.0	3.0
V	90.0	28.0	137.0	189.0	169.0	22.0	64.0	83.0	19.0	172.0	32.0
Cr	150.0	<10	60.0	60.0	50.0	10.0	50.0	<10	10.0	60.0	20.0
Co	30.0	2.0	16.0	28.0	23.0	1.0	13.0	7.0	3.0	22.0	4.0
Ni	99.0	1.0	21.0	51.0	43.0		21.0		2.0	41.0	5.0
Cu	29.0	20.0	100.0	229.0	122.0	2.0	17.0	17.0	7.0	72.0	688.0
Zn	129.0	29.0	111.0	107.0	109.0	11.0	59.0	61.0	25.0	109.0	12.0
Ga	18.6	17.0	21.5	20.0	20.5	14.6	17.2	18.8	14.8	23.2	11.6
As	26.0	5.0	11.0	5.0	5.0	5.0	5.0	11.0	6.0	7.0	6.0
Rb	71.1	97.9	67.4	26.2	48.6	87.6	33.0	111.0	179.0	35.6	53.5
Sr	130.5	77.0	423.0	312.0	398.0	41.1	396.0	354.0	25.5	465.0	141.5
Y	28.5	24.3	26.0	28.4	28.7	26.3	16.4	28.8	30.7	25.6	38.3
Zr	270.0	183.0	339.0	251.0	270.0	152.0	191.0	278.0	158.0	303.0	1040.0
Nb	27.0	16.0	18.7	16.9	18.9	15.9	6.5	12.4	15.0	22.7	38.3
Mo		1.0	1.0	1.0	1.0			2.0	1.0		2.0
Sn	2.0	1.0	2.0	1.0	2.0	2.0	1.0	2.0	1.0	2.0	2.0
Cs	0.74	0.52	0.49	0.31	0.42	0.93	0.21	1.55	1.57	0.27	0.18
Ba	394	1060	651	314	457	418	562	955	780	549	292
La	40.1	41.8	43.0	27.2	34.6	44.9	21.0	37.5	64.2	33.6	50.3
Ce	84.1	78.7	87.8	58.4	73.2	83.8	40.6	71.8	117.5	71.4	101.0
Pr	10.2	8.5	10.1	7.1	8.7	9.1	4.7	8.2	11.9	8.4	11.3
Nd	41.4	29.1	35.9	27.8	33.9	29.9	19.6	30.3	40.6	34.0	39.2
Sm	8.20	5.43	6.78	6.06	6.82	5.19	3.86	5.71	6.49	6.44	7.22
Eu	2.36	0.68	1.64	1.76	1.90	0.65	1.26	1.27	0.87	1.96	0.77
Gd	7.39	4.02	6.14	6.40	5.95	4.36	3.44	5.36	5.62	6.21	7.04
Tb	1.06	0.60	0.82	0.92	0.87	0.65	0.53	0.80	0.86	0.88	1.17
Dy	5.62	3.75	4.93	5.44	5.36	3.94	3.02	4.75	5.14	5.14	7.38
Ho	1.00	0.80	0.99	1.10	1.00	0.83	0.63	0.96	0.99	0.95	1.42
Er	2.66	2.25	2.68	3.05	2.85	2.45	1.62	3.00	2.77	2.45	4.20
Tm	0.39	0.38	0.37	0.40	0.36	0.35	0.23	0.43	0.45	0.39	0.62
Yb	2.20	2.59	2.44	2.75	2.49	2.63	1.44	3.16	2.74	2.15	4.02
Lu	0.35	0.40	0.38	0.39	0.39	0.45	0.22	0.48	0.47	0.32	0.60
Hf	5.7	5.3	7.9	5.9	5.5	4.6	4.7	7.1	4.9	6.6	22.7
Ta	1.5	0.9	1.1	1.0	1.1	1.0	0.4	0.7	0.9	1.4	2.4
W	2.0	2.0	1.0	2.0		3.0	3.0	2.0	2.0	3.0	2.0
Tl	0.0		10.0	0.0	0.0	0.0	10.0	0.0	10.0	10.0	0.0
Pb	32.0	0.0	0.0	0.0	0.0	0.0	0.0	8.0	4.0	0.0	6.0
Th	4.11	13.10	7.20	3.82	5.32	10.90	2.68	9.20	12.20	5.66	17.05
U	0.62	3.19	1.20	0.67	1.13	1.88	0.56	1.94	2.12	1.26	2.78
Eu/Eu*	0.93	0.45	0.78	0.86	0.91	0.42	1.06	0.70	0.44	0.95	0.33
(La/Yb) _N	12.29	10.88	11.88	6.67	9.37	11.51	9.83	8.00	15.80	10.54	8.44
(La/Sm) _N	3.08	4.84	3.99	2.82	3.19	5.44	3.42	4.13	6.22	3.28	4.38
(Gd/Yb) _N	2.71	1.25	2.03	1.88	1.93	1.34	1.93	1.37	1.66	2.33	1.41
Ba/Nb	14.59	66.25	34.81	18.58	24.18	26.29	86.46	77.02	52.00	24.19	7.62
ΣREE	207.03	179.02	203.97	148.75	178.38	189.18	102.17	173.67	260.60	174.24	236.19

Eu/Eu*: europium anomaly.

Table 4a. Major oxides of the La Quinta Formation igneous rocks. Values are expressed in wt.%. Geochemical classification following Middlemost (1994) and Pearce (1996).

Sample	1163	1167	1223	1224	1225	1227	1231	1232	1234	1236	1237
Classification	AB	R	BA	BA	M	R	D	A	R	TA	AR
SiO ₂	49	75.6	58.3	53	54.8	75.6	64	66.1	77.7	57.5	73.6
TiO ₂	1.84	0.2	1.05	1.17	1.32	0.17	0.64	0.56	0.18	1.31	0.47
Al ₂ O ₃	14.35	13.15	16.4	16.8	17	11.85	15.45	16	12.65	16.6	11.85
Fe ₂ O ₃ *	9.8	1.67	7.06	9.14	9	0.88	5.14	4.27	1.51	8.21	2.64
MnO	0.15	0.04	0.11	0.15	0.15	0.03	0.07	0.09	0.08	0.14	0.03
MgO	1.88	0.23	2.9	4.31	4.13	0.71	1.33	1.07	0.24	3.46	0.11
CaO	8.42	0.23	5.03	6.72	5.93	0.42	1.19	2.35	0.14	6.18	4.05
Na ₂ O	4.67	3.6	3.88	3.39	4.26	2.67	6.66	4.01	0.86	3.69	4.02
K ₂ O	2.53	4.94	2.14	1.06	1.72	4.66	2.02	3.86	6.57	1.52	2.88
P ₂ O ₅	0.6	0.03	0.49	0.41	0.5	0.03	0.23	0.18	0.02	0.58	0.06
LOI	7.43	0.91	2.49	1.86	2.6	1.8	1.71	3.1	1.63	1.23	0.84
Total	100.67	100.6	99.85	98.01	101.41	98.82	98.44	101.59	101.58	100.42	100.55

A: andesite, AB: alkali basalt, AR: alkali rhyolite, BA: basaltic andesite, D: dacite, M: monzodiorite, R: rhyolite, TA: trachyandesite.

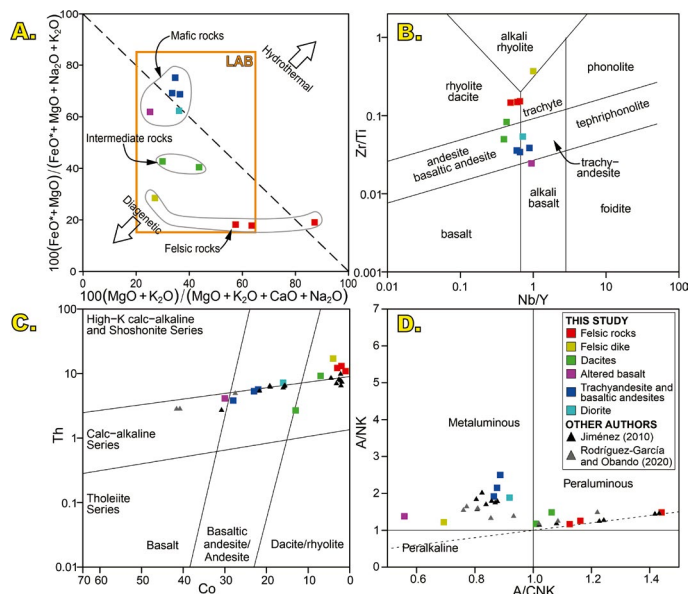


Figure 8. Geochemical classification diagrams for the La Quinta Formation igneous rocks. A. Alteration box plot (Large et al., 2001), where major oxides are expressed in wt.%. LAB: least altered box. B. Nb/Y vs. Zr/Ti (Pearce, 1996). C. Co vs. Th in ppm (Hastie et al., 2007). D. Shand's index after Maniar and Piccoli (1989).

In chondrite normalized (Boynton, 1983) rare earth element (REE) diagrams (Figure 10), the mafic samples ($\Sigma\text{REE} = 148\text{--}207$ ppm) have enrichments in light REE (LREE) with respect to heavy REE (HREE) ($\text{La}/\text{YbN} = 6.6\text{--}11.8$) and slightly fractionated HREE patterns ($\text{GdN}/\text{YbN} = 1.8\text{--}2.7$), and also agree well with basaltic trachyandesites, trachyandesites and andesites reported by Jiménez (2010) and Rodríguez-García & Obando (2020). Europium anomalies (Eu/Eu^*) in these rocks are insignificant ($\text{Eu}/\text{Eu}^* = 0.7\text{--}0.9$) and it predominates a general flat pattern, indicating that plagioclase

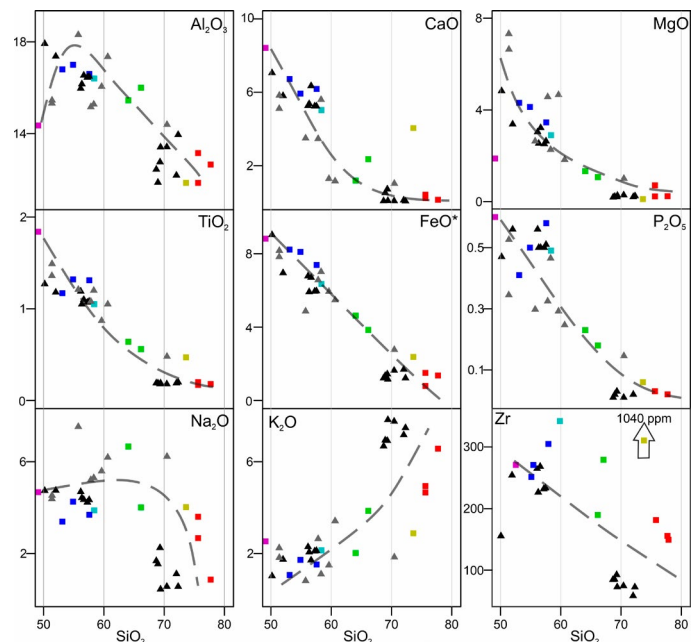


Figure 9. Harker diagrams of the La Quinta Formation igneous rocks. Symbols are the same as in Figure 8. The discontinuous dark grey line represents the general tendency of the data. Oxides are expressed in wt.% and Zr in ppm.

fractionation was not important in this stage (Winter, 2014). Mafic rocks are also enriched in large ion lithophile elements (LILE) compared to high field strength elements (HFSE), and in primitive mantle normalized diagrams display negative Nb and Ti tendencies and positive Pb and K tendencies (Figure 10). The distinctive positive Pb anomaly observed in the altered basalt is also present in the samples analyzed by Jiménez (2010) and Rodríguez-García & Obando (2020). Altogether, these geochemical features are common in subduction-related magmatism (Gill, 2010).

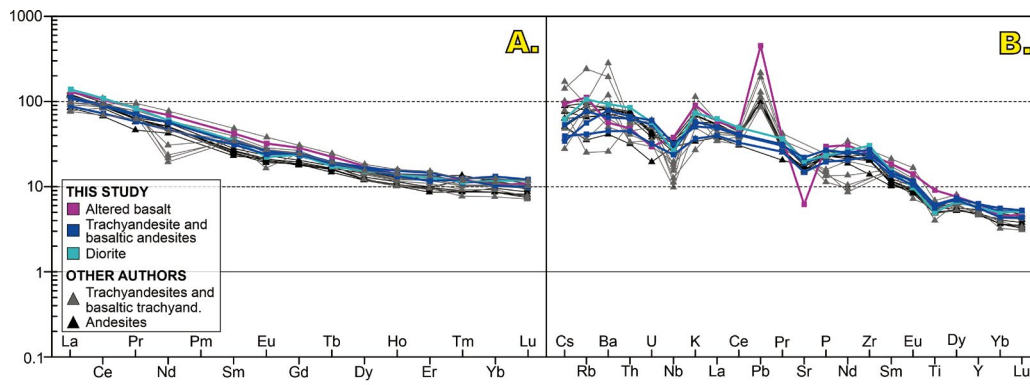


Figure 10. Trace element geochemical diagrams for the La Quinta Formation mafic rocks. A. Chondrite normalized (Boynnton, 1983) REE plots. B. Primitive mantle normalized multi-element plots (Sun & McDonough, 1989). Samples from Jiménez (2010) and Rodríguez-García & Obando (2020) are included.

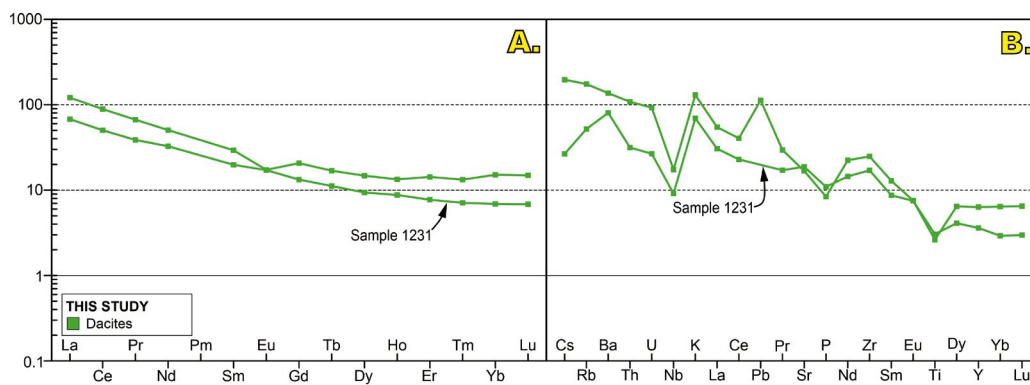


Figure 11. Trace element geochemical diagrams for the La Quinta Formation intermediate rocks. A. Chondrite normalized (Boynnton, 1983) REE plots. B. Primitive mantle normalized multi-element plots (Sun & McDonough, 1989).

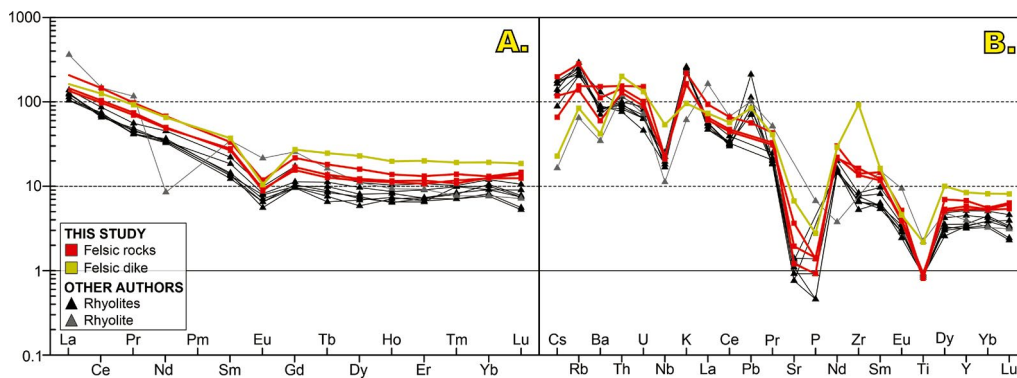


Figure 12. Trace element geochemical diagrams for the La Quinta Formation felsic rocks. A. Chondrite normalized (Boynnton, 1983) REE plots. B. Primitive mantle normalized multi-element plots (Sun & McDonough, 1989). Samples from Jiménez (2010) and Rodríguez-García & Obando (2020) are included.

The studied intermediate rocks exhibit total REE values ranging from 102.2 to 173.7 ppm. As depicted in the chondrite normalized diagram presented in Figure 11, dacites have higher concentrations of LREE compared to HREE (LaN/YbN = 8.0-9.8) and display rather fractionated HREE patterns (GdN/YbN = 1.4-1.9). Eu anomaly in the sample 1231 is absent (Eu/Eu* = 1.0) whereas in the sample 1232 is moderate negative (Eu/Eu* = 0.7); thus, in the former case, plagioclase fractionation was not remarkable, probably caused by early crystallization of amphibole as indicated by the listric-shaped HREE pattern (Figure 11) (Richards & Kerrich, 2007). Moreover, dacites are enriched in LILE with respect to HREE and show positive Pb and K anomalies as well

as negative Nb, P and Ti anomalies. Overall, these patterns are typically found in supra-subduction arcs (Gill, 2010; Winter, 2014).

Finally, felsic rocks hold the highest total amounts of REE (179.0-260.6 ppm) and have negative slope (LaN/YbN = 8.4-15.8) parallel patterns in the chondrite normalized REE diagram (Figure 12), with moderate MREE (medium REE) fractionation trends compared to LREE (LaN/SmN = 4.4-6.2) and flat HREE patterns (GdN/YbN = 1.3-1.7). Moderate-to-strong negative Eu anomalies (Eu/Eu* = 0.3-0.4) are present in all the samples of this group, defining a “seagull” profile and evidencing prolific plagioclase fractionation (Winter, 2014). In primitive mantle normalized spidergrams, analyzed rhyolites

and the ignimbrite exhibit contrasting geochemical characteristics when plotted along the felsic dike. In one hand, rhyolitic rocks are enriched in LILE compared to HFSE ($Ba/Nb = 26-66$) and are characterized by a positive K anomaly and deeply negative Nb, Sr, P and Ti anomalies (Figure 12). On the other hand, the dike has minor LILE (e.g., Cs, Rb, Ba) concentrations although maintain a relative enrichment of these elements compared to HFSE ($Ba/Nb = 7.6$); also, this sample has positive Th, Pb and Zr tendencies along with negative Nb, Sr, P and Ti tendencies. All these geochemical features are found in subduction related igneous rocks (Gill, 2010) and are very similar to those reported by Jiménez (2010) and Rodríguez-García & Obando (2020) for rhyolites from the La Quinta Formation.

5. Discussion

Petrogenesis of the igneous rocks from the La Quinta Formation

The La Quinta Formation comprises a thick succession of volcano-sedimentary rocks that is extensively exposed in the Serranía del Perijá and the Mérida Andes (Champetier de Ribes et al., 1961; Radelli, 1961; Forero, 1972; Maze, 1984; Montaña, 2009; Gómez et al., 2010; Jiménez, 2010; Ortega et al., 2012; González-Iregui et al., 2015; van der Lelij et al., 2016a; López-Isaza & Zuluaga, 2020; Rodríguez-García & Obando, 2020). The igneous part of this unit is formed of volcanoclastic, volcanic, plutonic and, probably, hypabyssal rocks with variable compositions (basaltic to rhyolitic), commonly displaying diagnostic geochemical features of supra-subduction magmatism that was transitional between calc-alkaline and alkaline. Harker diagrams (Figure 9) depict negative fractionation trends in compatible elements in response to the early crystallization of Ca-plagioclase, clinopyroxene, Fe-Ti oxides, olivine and apatite, as well as positive profiles in K_2O defining the late crystallization of alkali feldspar (sanidine); zirconium also depict a negative profile with increasing SiO_2 , probably due to the early fractionation of fine-grained zircon or baddeleyite. Fractionation of these minerals was also interpreted from spidergrams (Figure 10-12), where progressively deeper negative anomalies in Ti, Sr, Eu, Zr and P with increasing SiO_2 are present. High crystallization temperatures obtained for clinopyroxene (ca. 1120 °C) and magnetite-ilmenite (700-736 °C) from a basaltic andesite (sample 1224) also support this trend of differentiation, although suggest that Fe-Ti oxides arrived later than clinopyroxene to the paragenesis.

Notwithstanding the fact that amphibole was only observed in one dacite (sample 1231) and the monzodiorite, the decrease in Dy/Yb ratios with respect to SiO_2 (Figure 13B) indicates that crystallization of this mineral was remarkable during differentiation. Moreover, the presence of amphibole and biotite in some samples (Table 2) accounts for significant water contents in the magmas (Frost and Frost, 2014; Loucks, 2014), consistent with the co-crystallization of magnetite-ilmenite and magnetite-hematite in mafic and intermediate rocks, respectively, implying that parental magmas were oxidized (fO_2 varied between +1.2 Ni-NiO and magnetite-hematite buffers) as it is classically found in arc-magmas (Ishihara, 1977).

Low Th/Hf and Ta/Hf ratios (Figure 13C) in the mafic and intermediate rocks suggest a hybrid signature between arc and intraplate, as well as limited contribution from calc-alkaline or enriched mantle sources. However, rhyolites and the ignimbrite display a greater influence of a calc-alkaline reservoir, probably acquired during assimilation of older arcs (e.g., Paleozoic granitoids) (Maze, 1984; van der Lelij et al., 2016a; van der Lelij et al., 2019). On the other hand, andesites and rhyolites studied by Jiménez (2010) have an intraplate affinity and perhaps had a more enriched source or higher degrees of middle-to-upper crustal contamination. In fact, in the Th/La vs. Ba/La plot (Figure 13D), the samples define a gently sloped positive trend that is suggestive of higher crustal contamination in the most siliceous rocks, as it is also suggested by their peraluminous character (Figure 8D). This agrees with Maze (1984) and van der Lelij et al. (2019), who obtained values of $87Sr/86Sr$ (0.706-0.711) and eHf (-5.76) in volcanic rocks from the La Quinta Formation in the eastern flank of the Serranía del Perijá and the Mérida Andes, indicative of conspicuous crustal assimilation. In addition, the low variation in Ba/La ratios points toward inconstant influence of slab-derived fluids; although Pb positive tendencies found in most rocks (Figure 10-12) mark the incorporation of crustal derived sediments via subduction recycling (Wilson, 1989; Class et al., 2000; Sen, 2014; Winter, 2014).

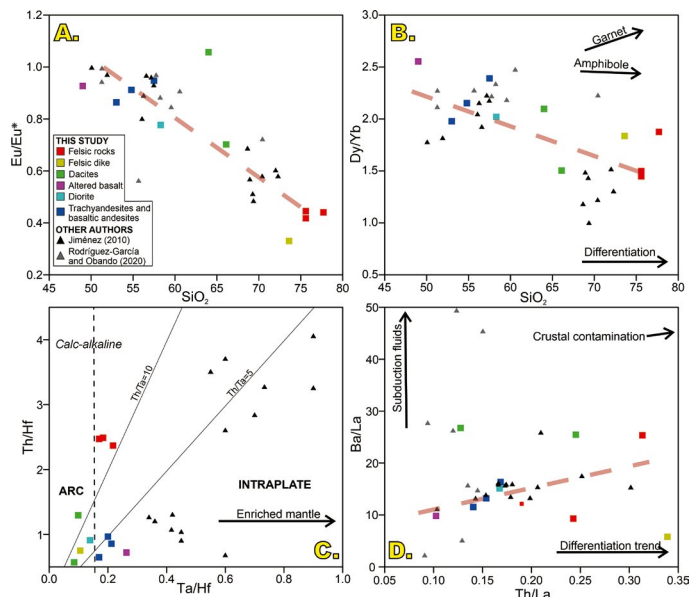


Figure 13. Petrogenetic geochemical diagrams for the igneous rocks from La Quinta Formation. A. SiO_2 vs. Eu/Eu^* . B. SiO_2 vs. Dy/Yb . C. Ta/Hf vs. Th/Hf . D. Th/La vs. Ba/La . SiO_2 concentration is expressed in wt.%.

It is worth noting that the sample 1231 lies in the adakite/TTG field (Martin, 1986) (Figure 14) and exhibits most of the adakite diagnostic geochemical characteristic (e.g., Richards and Kerrich, 2007), including: $SiO_2 > 56$ wt.% (64 wt.%), $Na_2O > 3.5$ wt.% (6.6 wt.%), $K_2O < 3.0$ wt.% (2.0 wt.%), $Rb < 65$ ppm (33 ppm), $Sr > 400$ ppm (396 ppm), $Y < 18$ ppm (16.4 ppm), $Yb < 1.9$ ppm (1.4 ppm), $Ni > 20$ ppm (21 ppm), $Cr > 30$ ppm (50 ppm), $Sr/Y > 20$ (24.1) and $Mg\#$ ca. 0.5 (0.4). Similarly, some of the volcanic rocks studied by Jiménez (2010) and Rodríguez-García & Obando (2020) display adakitic signatures as well.

In the original definition of “adakite”, Kay (1978) and Defant & Drummond (1990) stated that partial melting of hot and young garnet-bearing oceanic crust (eclogite-facies metamorphism) produced the anomalous high values in Sr/Y and La/Yb found in volcanic rocks from the Adak Island (Aleutians Arc). However, Kay and Kay (2002) later proposed that magmas with such signatures would also be a consequence of melting: 1) the base of the continental crust or 2) lower crustal slices driven to great depths by subduction erosion processes; in both cases, stabilizing garnet in the source. Additionally, Richards and Kerrich (2007) and Loucks (2014) demonstrated that adakitic geochemical features can also be acquired by different magmatic suites via extensive amphibole fractionation combined with limited early crystallization of plagioclase. Hence, we propose that the adakitic characteristics observed in the studied rocks are a consequence of differentiation processes (e.g., Richards & Kerrich, 2007; Loucks, 2014), having into account that the scarce adakite-like rocks in the study zones are spatially and genetically related to “normal” arc magmas (Figure 14) and that differentiation was strongly influenced by the fractionation of amphibole (Figure 13B).

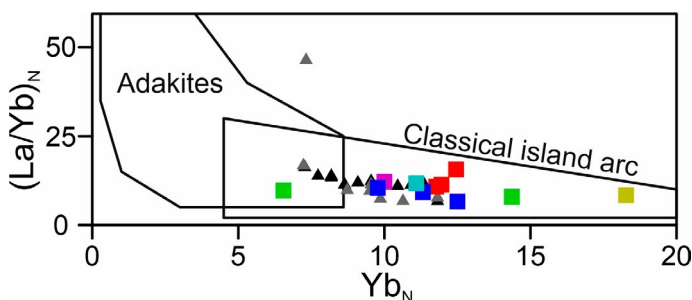


Figure 14. Adakite discrimination diagram of Martin (1986). Symbols are the same as in Figure 8.

Some typical adakitic indexes (e.g., Sr/Y and La/Yb) have arisen as powerful tools to evaluate periods of crustal thickening and thinning in orogens (Chapman et al., 2015; Chiaradia, 2015; Profeta et al., 2015; Chavarria et al., 2021). After selecting idoneous rocks for calculations following Chapman et al. (2015) and Profeta et al. (2015), three of the samples analyzed here (1231, 1223 and 1236) and some andesites studied by Jiménez (2010) yielded Sr/Y (14.0-24.1) and (La/Yb)_N (9.8-14.0) ratios equivalent to crustal thicknesses of 26-49 km (Profeta et al., 2015). These values indicate that the crust was normal to moderately thick and match the interval of ca. 30-60 km calculated by Ramírez et al. (2020) and Chavarria et al. (2021) in Jurassic plutonic and volcanic rocks from the Sierra Nevada de Santa Marta, which was situated trenchward with respect to the Machiques transtensional basin at that time (Bartok et al., 2015; Nova et al., 2019; Bayona et al., 2020; Ramírez et al., 2020). Moreover, these values are supported by middle-crustal clinopyroxene crystallization pressures of ca. 18 km that might mark the level at which initial (high-temperature) fractional crystallization took place.

Melting conditions in the source

The volcanic rocks from the La Quinta Formation are transitional between alkaline and calc-alkaline series, as shown by geochemical (Figure 8B-C) and mineralogical features (e.g., abundant sanidine in evolved rocks). These characteristics can result from assimilation/fractional crystallization, partial melting, source enrichment or a combination of all (Box & Flower, 1989). As previously mentioned, crustal assimilation was indeed significant and might explain, at least in part, the alkalinity of the rocks. On the other hand, low degrees of partial melting of the source can greatly enrich magmas in incompatible elements and is considered one of the main processes that rise alkalinity in subduction-related settings (Box & Flower, 1989). However, distinguishing between the effects of partial melting from those generated by source enrichments require complementary isotopic studies.

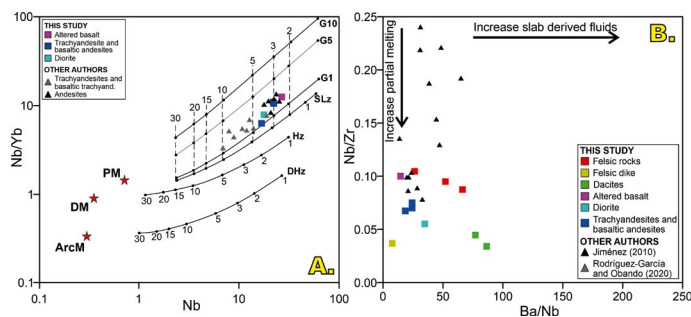


Figure 15. A. Nonmodal batch melting using the system Nb-Yb for mafic rocks from the La Quinta Formation (Safonova et al., 2016). B. Ba/Nb vs. Nb/Zr plot.

In order to evaluate the types of mantle sources and degrees of melting that produced the parental magmas of less differentiated rocks (mafic group), we employed a source-melting model constructed by Safonova et al. (2016) (Figure 15A), which assumes nonmodal batch melting using the system Nb-Yb. In this model, our samples and those presented by Jiménez (2010) and Rodríguez-García & Obando (2020) suggest up to 10% of melting of two probable sources: a peridotite containing 1% of garnet or a spinel lherzolite. In the former case, the presence of garnet as a residual phase in the source would generate steep negative slopes in HREE (Richards & Kerrich, 2007), contrasting with the dominant flat or listric-shaped HREE profiles depicted in the spiderplots (Figure 10-12). In this way, a spinel lherzolite is a better candidate for the main source of the magmas. Besides, our samples exhibit higher degrees of melting than the rhyolites studied by Jiménez (2010) (Figure 15B) explaining the “less enriched” character of the source indicated by Ta/Hf ratios (Figure 13C).

Hydrothermal alteration and Cu mineralization

The La Quinta Formation volcanic rocks sometimes display calc-silicate hydrothermal alteration in association with Cu mineralization (Figure 3D, 4F) (Jiménez, 2010; Ortega et al., 2012; UNAL-SGC, 2014, 2020; González-

Duran et al., 2017). The assemblage is constituted by variable amounts of quartz, pistacite, zoisite-clinozoisite, prehnite, carbonates, hydrated garnet (Adr70Grs30) and Ca-zeolites (Figure 4F). Given that hydrated garnets are stable at ca. 250-300 °C and well-crystallized epidote at >220-250 °C (Corbett & Leach, 1997; and references therein) and carbonates are commonly associated with them (Figure 5C-D), we interpret that the mineralizing fluids had mid-temperature and neutral-to-alkaline pH.

Although garnet is typically found in skarns due to elevated temperature metasomatism of calcareous protoliths (Meinert et al., 2005), the presence of garnet is also common in the deeper portions of Cu porphyries (Sillitoe, 2010) and IOCG clan of deposits (Corriveau, 2007). Nevertheless, there is neither field nor laboratory evidence that supports the presence of such magmatic-hydrothermal deposits in the study zones. In fact, Cu occurrences are normally stratabound and are related to specific basaltic horizons and green sandstones with plant remains, and hence several authors have preliminarily classified them as sediment-hosted stratiform copper systems (Wokittel & Restrepo-Acevedo, 1955; Champetier de Ribes et al., 1961; Radelli, 1961; Pagnacco, 1962; Rodríguez, 1986; Jiménez, 2010; Ortega et al., 2012; González-Duran et al., 2017). Hitzman et al. (2005) explained that the volcanic red-bed copper subtype is formed in rift-fill volcano-sedimentary sequences that have undergone various stages of diagenesis and/or burial metamorphism (epidote-prehnite/pumpellyite facies), by low-to-moderate temperature mineralizing fluids 50-400 °C. This deposit model partly matches several features found in Cu mineralization hosted in the La Quinta Formation and, perhaps, such hydrothermal fluids caused the calc-silicate alteration that preferably affects volcanic horizons and is sometimes associated to the ores.

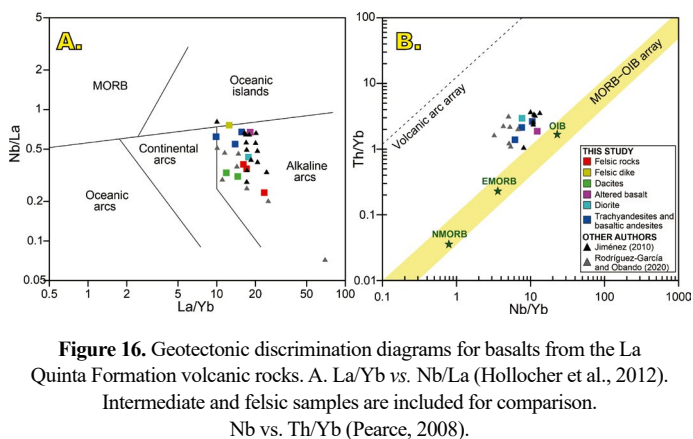


Figure 16. Geotectonic discrimination diagrams for basalts from the La Quinta Formation volcanic rocks. A. La/Yb vs. Nb/La (Hollocher et al., 2012). Intermediate and felsic samples are included for comparison. B. Nb vs. Th/Yb (Pearce, 2008).

Tectonic model and regional implications

As previously mentioned, the La Quinta Formation volcanics display several diagnostic features of supra-subduction magmatic rocks, such as: 1) early crystallization of Fe-Ti oxides and Ca-clinopyroxene along with extensive plagioclase and amphibole fractionation; 2) high LILE/HFSE and LREE/HREE ratios; 3) negative Nb and Ti tendencies combined with positive Pb tendencies; 4) co-crystallization of magnetite-ilmenite and magnetite-hematite defining oxidizing conditions (+1.2 Ni-NiO to magnetite-hematite buffers); and 5) peraluminous to metaluminous character. Additionally, uninterrupted patterns in Harker diagrams and sub-parallel profiles in REE spiderplots suggest that they indeed constitute a magmatic suite genetically linked.

In the discrimination diagram of Hollocher et al. (2012) for basalts, all the samples (differentiated rocks included for comparison) plot in the “Alkaline arcs” field (Figure 16A), in agreement with trace element classification schemes (Figure 8B-C). Likewise, the mafic rocks plot above the MORB-OIB array (high Th and Nb) (Figure 16B), which is normally found in arc-related rocks subjected to interaction with the continental crust during ascent (Pearce, 2008), consistent with isotopic ratios (Maze, 1984; van der Lelij et al., 2019). Combined, both diagrams define two features commonly found in early stages of continental rifting: alkaline tendencies and contamination by a thick continental crust (Winter, 2014).

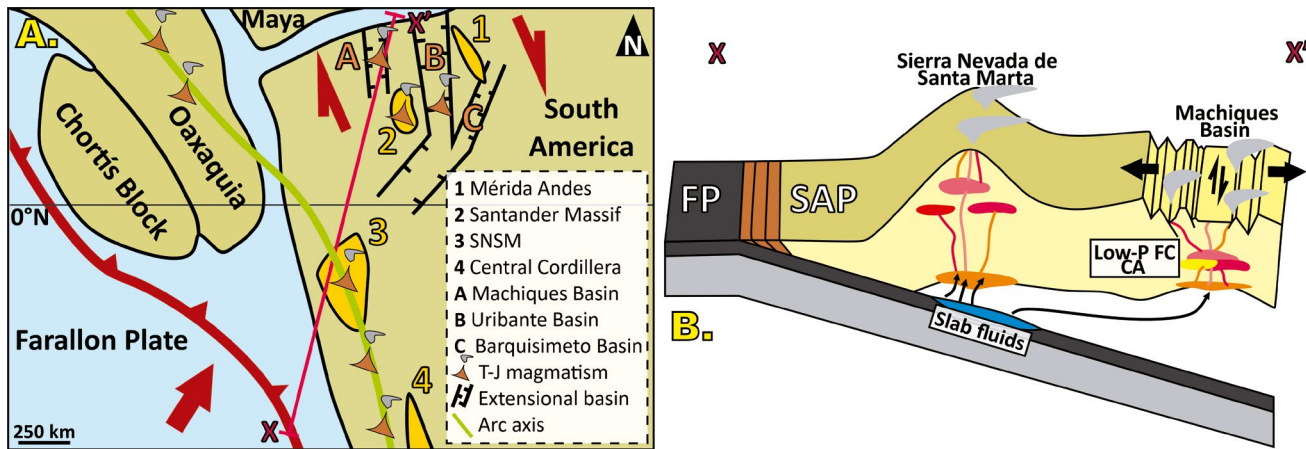


Figure 17. Proposed tectonic model to explain the generation of the igneous rocks from the La Quinta Formation. A. Reconstruction for the Lower to Middle Jurassic according to Nova et al. (2019), depicting the position of the continental arc axis with respect to the transtensional basins (Machiques, Uribante and Barquisimeto) in northwestern Gondwana, resulting from the break-up of Pangea. The red arrow indicates the dominant subduction trend and red half arrows depict the right-lateral sense of shearing. B. Schematic cross section X-X' showing the proposed hybrid tectonic scenario responsible for the La Quinta igneous rocks. In this model, the calc-alkaline to alkaline volcanic (>plutonic) activity that focused on the Machiques transtensional basin (La Quinta Formation) was somehow controlled by the influx of slab-derived fluids from the subducting Farallon Plate and hence records clear arc signatures. Nevertheless, low degrees of partial melting or the presence of a more enriched mantle source rose alkalinity of these rocks. During ascent, magmas underwent low-pressure (amphibole- and plagioclase-dominated) fractional crystallization (FC) and crustal assimilation (CA) in the middle crust, before erupting along major normal faults. Moreover, a coeval subduction-related continental arc formed to the SW and is represented by volcanic and plutonic rocks from the Sierra Nevada de Santa Marta. Modified from Martini & Ortega-Gutiérrez (2018) and Ramírez et al. (2020). FP: Farallon plate, SAP: South American Plate.

Following the abovementioned, the igneous rocks of the La Quinta Formation in the western flank of the Serranía del Perijá, northern Colombia, were formed in a paleo-subduction setting where the Farallon/Pacific plate was sinking beneath South America (Figure 17) (Bartok et al., 2015; Nova et al., 2019; Bayona et al., 2020). This processes generated Jurassic (*ca.* 163–191 Ma) volcanic-plutonic activity in the Sierra Nevada de Santa Marta (arc axis) (Bartok et al., 2015; Nova et al., 2019; Ramírez et al., 2020) coeval with the magmatism (volcanic>plutonic) in the Machiques transtensional basin or the present-day Serranía del Perijá (*ca.* 165–188) (Jiménez, 2010; González-Iregui et al., 2015; Nova et al., 2019; Rodríguez-García & Obando, 2020). The source of this volcanism in the western Perijá range is unknown, although Maze (1984) proposed that the locus of felsic products were the normal faults that bound grabens.

Probably, the calc-alkaline to alkaline volcanism in the Machiques basin resulted from the superposition of Farallon subduction and contemporaneous widespread extension owing to the separation of North and South American plates, counterclockwise rotation of the Yucatán Block and seafloor spreading in the proto-Caribbean ocean (accretion of para-autochthonous terranes model in Bayona et al., 2020). Therefore, we propose that the La Quinta Formation volcanics were generated in a hybrid tectonic domain that resulted from the interaction of the convergence along the western margin of northwestern Gondwana and the intracontinental rifting associated with the break-up of Pangea.

In the western Mérida Andes (Uribante basin) (Figure 17), Langer et al. (2014) and van der Lelij et al. (2016a) obtained crystallization (TIMS, U-Pb zircon) and cooling ages (Ar-Ar plateau in biotite) of 229 ± 15 Ma and 200.4 ± 0.9 Ma, respectively, in the basal tuffs from the La Quinta Formation. During the Lower Jurassic, the Uribante basin was located east of the Machiques basin, indicating that the magmatism migrated westward as evidenced by younger volcanic ages in the Colombian Perijá range (*ca.* 163–191 Ma). After that, the arc axis progressively moved to the west into the Central Cordillera, where the oldest Jurassic plutonic rocks display an age of 189 Ma (Bustamante et al., 2010; van der Lelij et al., 2016b), leading to the termination of the volcanic activity in the Machiques basin (Spikings et al., 2019).

Van der Lelij et al. (2016b) proposed that such a migration in the magmatism was a consequence of slab rollback in the Farallon Plate, which also could have contributed to the widening of extensional and transtensional

basins formed by the globalized divergent regime that controlled the Jurassic sedimentation in northwestern Gondwana (Figure 17). Nevertheless, those basins should not be considered as back-arc basins since their development is not a direct consequence of the interaction of Farallon-Pacific and South American plates, but a response to a major plate rearrangement (Wilson, 1989; Martini & Ortega-Gutiérrez, 2018).

6. Conclusions

The latest Triassic-Jurassic magmatic record present in the La Quinta Formation, Serranía del Perijá (northeast Colombia), was developed in the Machiques transtensional basin and displays wide compositional variations from basaltic to rhyolitic, following a calc-alkaline to alkaline trend of differentiation. These rocks represent a cogenetic igneous suite constituted by variable amounts of plagioclase, augite, quartz, amphibole, biotite and sanidine, with zircon, apatite, magnetite and ilmenite as the main accessory phases. Calc-silicate hydrothermal alteration with hydrated andradite-grossular, zeolites and epidote is often linked to Cu mineralization that might belong to the sediment-hosted stratiform copper clan of deposits.

Geochemical features displayed by these rocks are diagnostic of subduction-related settings associated with low degrees of partial melting (or an enriched mantle source), where magmas ascended through a normal-to-thickened crust and underwent low-pressure fractional crystallization and different degrees of crustal assimilation. Such processes summed with the existence of a contemporaneous well-developed continental arc (Sierra Nevada de Santa Marta) located trenchward, allowed us to invoke a hybrid tectonic scenario related to the coeval subduction of the Farallon Plate underneath northwest Gondwana and the ongoing divergence of North and South American plates resulting from the break-up of Pangea.

Acknowledgments

This research was supported by the Universidad Nacional de Colombia and the Servicio Geológico Colombiano, project: “*Proyecto Metalogenético en Zonas de Interés del Territorio Colombiano*”, Cooperation Agreement No. 001 of 2015. We want to express our gratitude to the reviewers for their insightful comments that helped us improved the manuscript. We are also grateful to Dr. Colombo Tassinari, Dr. António Mateus, Dr. Natalia Pardo, Dr.

Ana Elena Concha and Ana María Correa for the guidance during the field and laboratory works.

7. Bibliography

- ALS-Chemex (2022). Geochemistry, schedule of services & fees.
- Bacon, C. R. & Hirschmann, M. M. (1988). Mg/Mn partitioning as a test for equilibrium between coexisting Fe-Ti oxides. *American Mineralogist*, 73, 57-61.
- Barrett, P. M., Butler, R. J., Novas, F. E., Moore-Fay, S. C., Moody, J. M., Clark, J. M. & Sánchez-Villagra, M. R. (2008). Dinosaur remains from the La Quinta Formation (Lower or Middle Jurassic) of the Venezuelan Andes. *Palaontologische Zeitschrift*, 82, 163-177. <https://doi.org/10.1007/BF02988407>
- Bartok, P., Mejía-Hernández, M. C. & Moyano, I. (2015). Paleogeographic constraints on middle-to late-Jurassic tectonic reconstruction of the Maya block of southern Mexico and equivalent strata of northwestern South America. *AAPG Memoir*, 108, 201-216. <https://doi.org/10.1306/13531937M1082953>
- Bayona, G., Bustamante, C., Nova, G. & Salazar, A. M. (2020). *Jurassic Evolution of the Northwestern Corner of Gondwana: Present Knowledge and Future Challenges in Studying Colombian Jurassic Rocks*. In: Gómez, J. & Pinilla-Pachón, A. O. (Eds.). *The Geology of Colombia, 2 (Mesozoic)*. Servicio Geológico Colombiano, Publicaciones Especiales 36, 171-207. <https://doi.org/10.32685/pub.esp.36.2019.05>
- Box, S. E. & Flower, M. F. J. (1989). Introduction to Special Section on Alkaline Arc Magmatism: Journal of Geophysical Research. *Solid Earth*, 94, 4467-4468. <https://doi.org/10.1029/JB094iB04p04467>
- Boynton, W. V. (1983). *Cosmochemistry of the rare earth elements: meteorite studies*. In: Henderson, P. (Editor). *Rare earth element geochemistry*. Elsevier Science Publisher, Amsterdam, The Netherlands, 63-114 p. <https://doi.org/10.1016/B978-0-444-42148-7.50008-3>
- Bustamante, C., Cardona, A., Bayona, G., Mora, A., Valencia, V. A., Gehrels, G. E. & Vervoort, J. (2010). Geocronología U-Pb LA-ICP-MS y correlación regional de las rocas intrusivas del Jurásico Medio del Macizo de Garzón, Valle Superior del Magdalena y la cordillera Central, sur de Colombia. *Boletín de Geología*, 32, 93-109.
- Carmichael, I. (1967). The iron-titanium oxides of salic volcanic rocks and their associated ferromagnesian silicates. *Contributions to Mineralogy and Petrology*, 14, 36-64. <https://doi.org/10.1007/BF00370985>
- Cediel, F. (2019). *Phanerozoic orogens of northwestern South America: Cordilleran-type orogens. Taphrogenic tectonics. The Maracaibo Orogenic Float. The Chocó-Panamá indenter*. In: Cediel, F. & Shaw, R. P. (Editors). *Geology and Tectonics of Northwestern South America: The Pacific-Caribbean-Andean Junction*: Springer Nature Switzerland, 3-95. https://doi.org/10.1007/978-3-319-76132-9_1
- Champetier de Ribes, G., Pagnacco, P., Radelli, L. & Weecksteen, G. (1961). Geología y mineralizaciones cupríferas de la Serranía de Perijá, entre Becerril y Villanueva (Departamento del Magdalena, Intendencia de La Guajira). *Servicio Geológico Colombiano historical archive*, report No. 1431.
- Chapman, J. B., Ducea, M. N., DeCelles, P. G. & Profeta, L. (2015). Tracking changes in crustal thickness during orogenic evolution with Sr/Y: An example from the North American Cordillera. *Geology*, 43, 919-922. <https://doi.org/10.1130/G36996.1>
- Chavarría, L., Bustamante, C., Cardona, A., & Bayona, G. (2021). Quantifying crustal thickness and magmatic temperatures of the Jurassic to Early Cretaceous North-Andean arc. *International Geology Review*, 1-21. <https://doi.org/10.1080/00206814.2021.1992301>
- Chiaradia, M. (2015). Crustal thickness control on Sr/Y signatures of recent arc magmas: An Earth scale perspective. *Scientific Reports*, 5(8115), 1-5. <https://doi.org/10.1038/srep08115>
- Class, C., Miller, D., Goldstein, S. & Langmuir, C. (2000). Distinguishing melt and fluid subduction components in the Umnak volcanic, Aleutian arc. *Geochemistry Geophysics Geosystems G3*, v. 1. <https://doi.org/10.1029/1999GC000010>
- Colmenares, F., Mesa, A. M., Roncancio, J., Arciniegas, E., Pedraza, P., Cardona, A., Romero, A. J., Silva, C. A., Alvarado, S., Romero, O. A. & Vargas, A. F. (2007). *Geología de las planchas 11, 12, 13, 14, 18, 19, 20, 21, 25, 26, 27, 33, 34 y 40. Proyecto: "Evolución geohistórica de la Sierra Nevada de Santa Marta"*. Ingeominas-Invenmar-Ecopetrol-ICP-Geosearch Ltda. Servicio Geológico Colombiano.
- Correa-Martínez, A. M., Rodríguez-García, G., Isabel Arango, M. & Zapata, G. (2019). Petrografía, geoquímica y geocronología U-Pb de las rocas volcánicas y piroclásticas de la Formación Noreán al NW del Macizo de Santander, Colombia. *Boletín de Geología*, 41, 29-54. <https://doi.org/10.18273/revbol.v41n1-2019002>
- Corriveau, L. (2007). Iron oxide copper-gold deposits: A Canadian perspective: Mineral Deposits of Canada: A Synthesis of Major Deposit-Types, District Metallogeny, the Evolution of Geological Provinces, and Exploration Methods. *Geological Association of Canada, Mineral Deposits Division, Special Publication*, 5, 307-328.
- Defant, M. J., & Drummond, M. S. (1990). Derivation of some modern arc magmas by melting of young subducted lithosphere. *Nature*, 347, 662-665. <https://doi.org/10.1038/347662a0>
- Forero, A. (1972). Estratigrafía del Precretácico en el flanco occidental de la Serranía de Perijá. *Geología Colombiana*, 7, 7-78.
- Frost, B. R. & Frost, C. D. (2014). *Essentials of Igneous and Metamorphic Petrology*. Cambridge University Press, Cambridge, UK, 303 pp. <https://doi.org/10.1017/9781108685047>
- Gill, R. (2010). *Igneous Rocks and Processes*. Wiley-Blackwell, Oxford, UK, 472 pp.
- Gómez, L., Buchely, F., Lancheros, J., Dávila, C., López, C., Romero, O. & González, F. (2010). *Cartografía geológica y muestreo geoquímico de la parte norte de la Serranía del Perijá planchas 21, 22, 27, 28, 34 y 35*. Servicio Geológico Colombiano. <https://doi.org/0.32685/10.143.2009.243>
- González-Duran, A., Cano, N., Molano, J. C., Guerrero, N., Sepúlveda, J., Prieto, D. & Tassinari, C. C. G. (2017). *Características geoquímicas de las mineralizaciones de cobre hospedadas en la Formación La Quinta*. XVI Colombian Geological Congress, Santa Marta, Colombia, 1706-1709.
- González-Iregui, H., Salinas-Echeverri, R., Cárdenas, J., Muñoz, C. & Vélez-Giraldo, W. (2015). *Geología de la plancha 41 - Becerril, escala 1:100.000, Memoria Explicativa*. Servicio Geológico Colombiano.
- GRP Ltda. (2010). *Geología de las planchas 27-Valledupar y 28-Villanueva, escala 1:100.000*. Servicio Geológico Colombiano.
- Hastie, A. R., Kerr, A. C., Pearce, J. A. & Mitchell, S. F. (2007). Classification of altered volcanic island arc rocks using immobile trace elements: Development of the Th-Co discrimination diagram. *Journal of Petrology*, 48, 2341-2357. <https://doi.org/10.1093/petrology/egm062>
- Hitzman, M., Kirkham, R., Broughton, D., Thorson, J., & Selley, D. (2005). *The sediment-hosted stratiform copper ore system*. In: Hedenquist, J. W., Thompson, J. F. H., Goldfarb, R. J., & Richards, J. P. (Eds.). *Society of Economic Geologists, One Hundredth Anniversary Volume*, 609-642. <https://doi.org/10.5382/AV100.19>
- Hollocher, K., Robinson, P., Walsh, E., & Roberts, D. (2012). Geochemistry of amphibolite-facies volcanics and gabbros of the Støren nappe in extensions west and southwest of Trondheim, western gneiss region, Norway: a key to correlations and paleotectonic settings. *American Journal of Science*, 312, 357-416. <https://doi.org/10.2475/04.2012.01>
- Invenmar, Ingeominas, Ecopetrol, ICP, and Geosearch (2007). *Geología de la Plancha 27-Agustín Codazzi, escala 1:100.000*. Servicio Geológico Colombiano.
- Ishihara, S. (1977). The magnetite-series and ilmenite-series granitic rocks. *Mining Geology*, 27, 293-305. <https://doi.org/10.11456/shigenchishitsu1951.27.293>
- Jiménez, C. A. (2010). *Vulcanismo y mineralizaciones cupríferas en la Serranía del Perijá*. B.Sc. Thesis, Facultad de Minas, Universidad Nacional de Colombia, Medellín, Colombia.

- Kay, R. W. (1978). Aleutian magnesian andesites: melts from subducted Pacific Ocean crust. *Journal of Volcanology and Geothermal Research*, 4, 117-132. [https://doi.org/10.1016/0377-0273\(78\)90032-X](https://doi.org/10.1016/0377-0273(78)90032-X)
- Kay, R. W. & Kay, S. M. (2002). Andean Adakites: Three ways to make them. *Acta Petrologica Sinica*, 18, 303-311.
- Kellogg, J. N. (1984). Cenozoic tectonic history of the Sierra de Perijá, Venezuela-Colombia, and adjacent basins. *Geological Society of America, Memoir*, 162, 239-261. <https://doi.org/10.1130/MEM162-p239>
- Klein, D. P. & Johnson, G. R. (1983). Density, Porosity, and Magnetic Properties of Rock Specimens from Southwestern Arizona. *United States Geological Survey, open-file report*, 83-808. <https://doi.org/10.3133/ofr83808>
- Langer, M. C., Rincón, A. D., Ramezani, J., Solórzano, A. & Rauhut, O. W. M. (2014). New dinosaur (Theropoda, stem-Averostra) from the earliest Jurassic of the La Quinta formation, Venezuelan Andes. *Royal Society Open Science*, 1(140184). <https://doi.org/10.1098/rsos.140184>
- Large, R. R., Gemmill, J. B. & Paulick, H. (2001). The alternation box plot: A simple approach to understanding the relationship between alteration mineralogy and lithochemistry associated with volcanic-hosted massive sulfide deposits. *Economic Geology*, 96, 957-971. <http://dx.doi.org/10.2113/96.5.957>
- Leal-Mejía, H. (2011). *Phanerozoic gold metallogeny in the Colombian Andes: A tectono-magmatic approach*. Ph.D. Thesis, Universitat de Barcelona, Barcelona, Spain.
- Leal-Mejía, H., Shaw, R. P. & Melgarejo i Draper, J. C. (2019). *Spatial-temporal migration of granitoid magmatism and the phanerozoic tectono-magmatic evolution of the Colombian Andes*. In: Cediél, F. & Shaw, R. P. (Editors). *Geology and Tectonics of Northwestern South America: The Pacific-Caribbean-Andean Junction*: Springer Nature Switzerland, p. 253-410. https://doi.org/10.1007/978-3-319-76132-9_5
- van der Lelij, R., Spikings, R., Ulianov, A., Chiaradia, M. & Mora, A. (2016a). Palaeozoic to Early Jurassic history of the northwestern corner of Gondwana, and implications for the evolution of the Iapetus, Rheic and Pacific Oceans. *Gondwana Research*, 31, 271-294. <https://doi.org/10.1016/j.gr.2015.01.011>
- van der Lelij, R., Spikings, R., and Mora, A. (2016b). Thermochronology and tectonics of the Mérida Andes and the Santander Massif, NW South America. *Lithos*, 248-251, 220-239. <https://doi.org/10.1016/j.lithos.2016.01.006>
- van der Lelij, R., Spikings, R., Gerdes, A., Chiaradia, M., Vennemann, T. & Mora, A. (2019). Multi-proxy isotopic tracing of magmatic sources and crustal recycling in the Palaeozoic to Early Jurassic active margin of North-Western Gondwana. *Gondwana Research*, 66, 227-245. <https://doi.org/10.1016/j.gr.2018.09.007>
- LeMaitre, R. W., Streckeis, A., Zanettin, B., Le Bas, M. J., Bonin, B., Bateman, P., Bellieni, G., Dudek, A., Efmova, S., Keller, J., Lameyre, J., Sabine, P. A., Schmid, R., Sorensen, H. & Woolley, A. R. (2002). *Igneous Rocks: A Classification and Glossary of Terms*. Cambridge University Press, Cambridge, UK, 253 pp. <https://doi.org/10.1017/CBO9780511535581>
- Lepage, L. D. (2003). ILMAT: An Excel worksheet for ilmenite-magnetite geothermometry and geobarometry. *Computers and Geosciences*, 29, 673-678. [https://doi.org/10.1016/S0098-3004\(03\)00042-6](https://doi.org/10.1016/S0098-3004(03)00042-6)
- López-Isaza, J. A. & Zuluaga, C. A. (2020). Late Triassic to Jurassic Magmatism in Colombia: Implications for the Evolution of the Northern Margin of South America: *Geology of Colombia*, 2, 77-116. <https://doi.org/10.32685/pub.esp.36.2019.03>
- López-Isaza, J. A. & Zuluaga, C. A. (2020). *Late Triassic to Jurassic magmatism in Colombia: Implications for the evolution of the northern margin of South America*. In: Gómez, J. & Pinilla-Pachon, A. O. (Editors). *The Geology of Colombia, Volume 2 Mesozoic*. Servicio Geológico Colombiano, Publicaciones Geológicas Especiales 36, p. 77-116. Bogotá. <https://doi.org/10.32685/pub.esp.36.2019.03>
- Loucks, R. R. (2014). Distinctive composition of copper-ore-forming arc magmas. *Australian Journal of Earth Sciences*, 61, 5-16. <https://doi.org/10.1080/08120099.2013.865676>
- Maniar, P. D. & Piccoli, P. M. (1989). Geological Society of America Bulletin Tectonic discrimination of granitoids. *Geological Society of America Bulletin*, 101, 635-643. [https://doi.org/10.1130/0016-7606\(1989\)101<0635:TDOG>2.3.CO;2](https://doi.org/10.1130/0016-7606(1989)101<0635:TDOG>2.3.CO;2)
- Martin, H. (1986). Effect of steeper Archean geothermal gradient on geochemistry of subduction-zone magmas. *Geology*, 14, 753-756. [https://doi.org/10.1130/0091-7613\(1986\)14<753:EOSAG>2.0.CO;2](https://doi.org/10.1130/0091-7613(1986)14<753:EOSAG>2.0.CO;2)
- Martini, M. & Ortega-Gutiérrez, F. (2018). Tectono-stratigraphic evolution of eastern Mexico during the break-up of Pangea: A review. *Earth-Science Reviews*, 183, 38-55. <https://doi.org/10.1016/j.earscirev.2016.06.013>
- Maze, W. B. (1984). Jurassic La Quinta Formation in the Sierra de Perijá, northwestern Venezuela: Geology and tectonics environment of the red beds and volcanic rocks. *Geological Society of America Memoir*, 162, 263-282. <https://doi.org/10.1130/MEM162-p263>
- Meinert, L. D., Dipple, G. M. & Nicolescu, S. (2005). World skarn deposits. *Society of Economic Geologists, One Hundredth Anniversary Volume*, 299-336. <https://doi.org/10.5382/AV100.11>
- Middlemost, E. (1994). Naming materials in the magma/igneous rock system. *Earth-Science Reviews*, 37, 215-224. [https://doi.org/10.1016/0012-8252\(94\)90029-9](https://doi.org/10.1016/0012-8252(94)90029-9)
- Mojica, J. & Kammer, A. (1995). Eventos Jurásicos en Colombia. *Geología Colombiana*, 19, 165-172.
- Montaño, P. (2009). *Caracterización petrográfica y geocronología detrítica de las rocas aflorantes en el arroyo Alberto (Serranía del Perijá), infrayacentes a la Formación Río Negro*. B.Sc. Thesis, Universidad Nacional de Colombia, Bogotá, Colombia, 20 pp.
- Morimoto, N. (1988). Nomenclature of Pyroxenes. *Mineralogy and Petrology*, 39, 55-76. <https://doi.org/10.1007/BF01226262>
- Nadoll, P., Angerer, T., Mauk, J. L., French, D. & Walshe, J. (2014). The chemistry of hydrothermal magnetite: A review. *Ore Geology Reviews*, 61, 1-32. <https://doi.org/10.1016/j.oregeorev.2013.12.013>
- Nimis, P. (1995). A clinopyroxene geobarometer for basaltic systems based on crystal-structure modeling. *Contributions to Mineralogy and Petrology*, 121, 115-125. <https://doi.org/10.1007/s004100050093>
- Nova, G., Bayona, G. A., Silva-Tamayo, J. C., Cardona, A., Rapalini, A., Montaño, P. C., Eisenhauer, A., Dussan, K. T., Valencia, V. A., Ramirez, V. & Montes, C. (2019). Jurassic break-up of the Peri-Gondwanan margin in northern Colombia: Basin formation and implications for terrane transfer. *Journal of South American Earth Sciences*, 89, 92-117. <https://doi.org/10.1016/j.jsames.2018.11.014>
- Ortega, C., Rojas-Martínez, E. & Manco-Jaraba, D. (2012). Mineralización de cobre en el sector de San Diego, Serranía del Perijá. *Geología Colombiana*, 37, 51-62.
- Ostos, M., Yoris, F. & Avé-Lallemant, H. (2005). Overview of the southeast Caribbean-South American plate boundary zone. *Geological Society of America Special Paper*, 394, 53-89. <https://doi.org/10.1130/0-8137-2394-9.53>
- Pagnacco, P. (1962). Cupriferous mineralizations in the Serranía de Perijá between Codazzi and Molino (Colombia). *Geología Colombiana*, 2, 5-13.
- Pearce, J. A. (1996). A User's Guide to Basalt Discrimination Diagrams. In: Wyman, D. A. (Ed.). *Trace Element Geochemistry of Volcanic Rocks: Applications for Massive Sulphide Exploration*, Geological Association of Canada, Short Course Notes, Vol. 12, 79-113.
- Pearce, J. A. (2008). Geochemical fingerprinting of oceanic basalts with applications to ophiolite classification and the search for Archean oceanic crust. *Lithos*, 100, 14-48. <https://doi.org/10.1016/j.lithos.2007.06.016>
- Profeta, L., Ducea, M. N., Chapman, J. B., Paterson, S. R., Gonzales, S. M. H., Kirsch, M., Petrescu, L. & DeCelles, P. G. (2015). Quantifying crustal thickness over time in magmatic arcs. *Scientific Reports*, 5, 1-7. DOI: 10.1038/srep17786

- Radelli, L. (1961). Acerca de la Serranía de Perijá entre Codazzi y Villanueva. *Geología Colombiana*, 1, 23-41.
- Ramírez, D. A., Correa-Martínez, A. M., Zapata-Villada, J. P. & Rodríguez-García, G. (2020). Tectono-magmatic implications of the Jurassic volcanic and volcanoclastic record of the Santa Marta Massif (Colombia). *Journal of South American Earth Sciences*, 104, 1-24. <https://doi.org/10.1016/j.jsames.2020.102866>
- Richards, J. P. & Kerrich, R. (2007). Adakite-like rocks: their diverse origins and questionable role in metallogenesis. *Economic Geology*, 102, 537-576. <https://doi.org/10.2113/gsecongeo.102.4.537>
- Rodríguez-García, G. (2018). Caracterización petrográfica, química y edad Ar-Ar de cuerpos porfídicos intrusivos en la Formación Saldaña. *Boletín Geológico*, 44, 5-23. <https://doi.org/10.32685/0120-1425/boletin-geo.44.2018.5>
- Rodríguez-García, G. & Obando, G. (2020). Volcanism of the La Quinta Formation in the Perijá mountain range. *Boletín Geológico*, 46, 51-94. <https://orcid.org/0000-0003-1422-3523>
- Rodríguez-García, G., Arango, M. I., Zapata, G. & Bermúdez, J. G. (2016). *Catálogo de unidades litoestratigráficas de Colombia - Formación Saldaña - Cordilleras Central y Oriental Tolima, Huila, Cauca y Putumayo*. Catálogos estratigráficos, Servicio Geológico Colombiano.
- Rodríguez-García, G., Arango, M. I., Zapata, G. & Bermúdez, J. G. (2018). Petrotectonic characteristics, geochemistry, and U-Pb geochronology of Jurassic plutons in the Upper Magdalena Valley-Colombia: Implications on the evolution of magmatic arcs in the NW Andes. *Journal of South American Earth Sciences*, 81, 10-30. <https://doi.org/10.1016/j.jsames.2017.10.012>
- Rodríguez, S. E. (1986). Génesis y mineralogía de los depósitos de cobre del Táchira Nororiental, Venezuela. *Geología Colombiana*, 15, 177-184.
- Rudnick, R. L. & Gao, S. (2003). *Composition of the continental crust*. In: Hollan, H. D. & Turekian, K. K. (Eds). *Treatise on Geochemistry*. Elsevier Inc., chapter 3.01, pp. 64. <https://doi.org/10.1016/B0-08-043751-6/03016-4>
- Saez-Paz, J. (2012). *Estudio al microscopio de 5 muestras del proyecto San Diego*. Internal report, Carboandes, Colombia.
- Safonova, I., Biske, G., Romer, R. L., Seltmann, R., Simonov, V. & Maruyama, S. (2016). Middle Paleozoic mafic magmatism and ocean plate stratigraphy of the South Tianshan, Kyrgyzstan. *Gondwana Research*, 30, 236-256. <https://doi.org/10.1016/j.gr.2015.03.006>
- Sen, G. (2014). *Petrology: Principles and practice*. Springer Nature Switzerland, pp. 370. <https://doi.org/10.1007/978-3-642-38800-2>
- Sillitoe, R. H. (2010). Porphyry copper systems. *Economic Geology*, 105, 3-41. <https://doi.org/10.2113/gsecongeo.105.1.3>
- Spikings, R. A., Cochrane, R., Vallejo, C., Villagomez, D., Van der Lelij, R., Paul, A. & Winkler, W. (2019). *Latest Triassic to Early Cretaceous tectonics of the Northern Andes: Geochronology, geochemistry, isotopic tracing, and thermochronology*. In: Horton, B. K. & Folguera, A. (Editors). *Andean Tectonics*. Elsevier Inc., 173-208. <https://doi.org/10.1016/B978-0-12-816009-1.00009-5>
- Sun, S. S. & McDonough, W. F. (1989). Chemical and isotopic systematics of oceanic basalts: Implications for mantle composition and processes. *Geological Society Special Publication*, 42, 313-345. <http://dx.doi.org/10.1144/GSL.SP.1989.042.01.19>
- Tschanz, C., Jimeno, A. & Cruz, B. J. (1969). *Geology of the Santa Marta area (Colombia)*. Instituto Nacional de Investigaciones Geológico-Mineras (Servicio Geológico Colombiano).
- UNAL-SGC (2014). *Caracterización metalogénica de zonas de interés para exploración mineral en áreas estratégicas en los Andes colombianos*. Cooperation Agreement No. 014 de 2013. Servicio Geológico Colombiano.
- UNAL-SGC (2020). *Informe final de la zona de San Diego-Perijá*. Special Cooperation Agreement No. 004 de 2019. Servicio Geológico Colombiano.
- Villagómez, D., Spikings, R., Magna, T., Kammer, A., Winkler, W. & Beltrán, A. (2011). Geochronology, geochemistry and tectonic evolution of the Western and Central cordilleras of Colombia. *Lithos*, 125, 875-896. <https://doi.org/10.1016/j.lithos.2011.05.003>
- Wang, X., Hou, T., Wang, M., Zhang, C., Zhang, Z., Pan, R., Marxer, F. & Zhang, H. (2021). A new clinopyroxene thermobarometer for mafic to intermediate magmatic systems. *European Journal of Mineralogy*, 33, 621-637. <https://doi.org/10.5194/ejm-33-621-2021>
- Whitney, D. L. & Evans, B. W. (2010). Abbreviations for names of rock-forming minerals. *American Mineralogist*, 95, 185-187. <https://doi.org/10.2138/am.2010.3371>
- Wilson, M. (1989). *Igneous Petrogenesis*. Springer, Dordrecht, The Netherlands, 480 pp. <https://doi.org/10.1007/978-94-010-9388-0>
- Winter, J. D. (2014). *Principles of igneous and metamorphic petrology*. Pearson Education Limited, Harlow, UK, 738 pp.
- Wokittel, R. & Restrepo-Acevedo, H. (1955). *Formación cuprífera de la Serranía del Perijá (intendencia de la Guajira y departamento del Magdalena). Geología de la Sierra Nevada de Santa Marta y Serranía de Perijá. Servicio Geológico Colombiano historical archive, report No. 1193*. <https://doi.org/10.32685/0120-1425/bolgeol5.3.1957.331>

